Correspondence to:
S. Moreau,
sebastien.moreau@utas.edu.au

Sea Ice Meltwater and Circumpolar Deep Water Drive Contrasting Productivity in Three Antarctic Polynyas

S. Moreau[1,2,3] (iD), D. Lannuzel[1,4], J. Janssens[1], M. C. Arroyo[5] (iD), M. Corkill[1] (iD), E. Cougnon[2,4,6] (iD), C. Genovese[1], B. Legresy[4,7], A. Lenton[4,7] (iD), V. Puigcorbé[8] (iD), L. Ratnarajah[4], S. Rintoul[4,7,9] (iD), M. Roca-Martí[10,11] (iD), M. Rosenberg[1,4] (iD), E. H. Shadwick[5,7] (iD), A. Silvano[1,4,7] (iD), P. G. Strutton[1,2,6] (iD), and B. Tilbrook[4,7] (iD)

[1]Institute for Marine and Antarctic Studies, University of Tasmania, Hobart, Tasmania, Australia, [2]Australian Research Council Antarctic Gateway Partnership, University of Tasmania, Hobart, Tasmania, Australia, [3]Fram Centre, Norwegian Polar Institute, Tromsø, Norway, [4]Antarctic Climate and Ecosystems Co-operative Research Centre, University of Tasmania, Hobart, Tasmania, USA, [5]Virginia Institute of Marine Science, College of William and Mary, Williamsburg, Virginia, USA, [6]Australian Research Council Centre of Excellence for Climate Extremes, University of Tasmania, Hobart, Tasmania, Australia, [7]Commonwealth Scientific and Industrial Research Organisation, Oceans and Atmosphere, Hobart, Tasmania, Australia, [8]School of Science and Centre for Marine Ecosystems Research, Edith Cowan University, Joondalup, Western Australia, Australia, [9]Centre for Southern Hemisphere Oceans Research, CSIRO, Hobart, Tasmania, Australia, [10]Institut de Ciència i Tecnologia Ambientals i Departament de Física, Universitat Autònoma de Barcelona, Bellaterra, Spain, [11]Woods Hole Oceanographic Institution, Woods Hole, Massachusetts, USA

Abstract In the Southern Ocean, polynyas exhibit enhanced rates of primary productivity and represent large seasonal sinks for atmospheric CO_2. Three contrasting east Antarctic polynyas were visited in late December to early January 2017: the Dalton, Mertz, and Ninnis polynyas. In the Mertz and Ninnis polynyas, phytoplankton biomass (average of 322 and 354 mg chlorophyll a (Chl a)/m^2, respectively) and net community production (5.3 and 4.6 mol C/m^2, respectively) were approximately 3 times those measured in the Dalton polynya (average of 122 mg Chl a/m^2 and 1.8 mol C/m^2). Phytoplankton communities also differed between the polynyas. Diatoms were thriving in the Mertz and Ninnis polynyas but not in the Dalton polynya, where *Phaeocystis antarctica* dominated. These strong regional differences were explored using physiological, biological, and physical parameters. The most likely drivers of the observed higher productivity in the Mertz and Ninnis were the relatively shallow inflow of iron-rich modified Circumpolar Deep Water onto the shelf as well as a very large sea ice meltwater contribution. The productivity contrast between the three polynyas could not be explained by (1) the input of glacial meltwater, (2) the presence of Ice Shelf Water, or (3) stratification of the mixed layer. Our results show that physical drivers regulate the productivity of polynyas, suggesting that the response of biological productivity and carbon export to future change will vary among polynyas.

1. Introduction

The oceans take up more than 25% of anthropogenic carbon dioxide (CO_2) emissions (Le Quéré et al., 2016), thereby mitigating climate change. The Southern Ocean is responsible for 40% of this anthropogenic CO_2 uptake by the oceans (Khatiwala et al., 2009; Sabine et al., 2004), a trend which has reinvigorated lately after receding between 2002 and 2012 (Landschützer et al., 2015). While the largest net sink is in the vast sub-Antarctic zone, on the northern flank of the Antarctic Circumpolar Current (Lenton et al., 2013; Sallee et al., 2012), considerable CO_2 uptake occurs in the continental shelf and coastal zone, including polynyas. For example, Arrigo, van Dijken, and Long (2008) estimated that CO_2 uptake in the Ross Sea was responsible for 27% of the total Southern Ocean CO_2 uptake.

The Southern Ocean CO_2 sink is due to a combination of circulation, temperature effects, and biological productivity. The response of the Southern Ocean and its biological pump to a changing climate will influence how much atmospheric CO_2 can be sequestered in the future (Constable et al., 2014; Sigman et al., 2010; Takahashi et al., 2009). The most biologically productive regions of the Southern Ocean are pelagic regions downstream of landmasses, the marginal ice zone, and the continental shelf and coastal zone, including polynyas (Ferreyra et al., 2004). The contribution of these regions to the total satellite-derived primary productivity of the Southern Ocean is 1.73 ± 0.06 Pg C/year for the open ocean,

0.16 ± 0.02 Pg C/year for the marginal ice zone, and 0.07 ± 0.01 Pg C/year for the continental shelf and coastal zone (Arrigo, van Dijken, & Bushinsky, 2008). Relative to its size, the coastal region is by far the most productive, with satellite-derived mean areal production of 109 g C m^{-2} yr^{-1} compared to 54 g C m^{-2} yr^{-1} for the open ocean and 58 g C m^{-2} yr^{-1} for the marginal ice zone (Arrigo, van Dijken, & Bushinsky, 2008). Because the average phytoplankton concentration in polynyas is more than double that of all open waters around Antarctica (Arrigo et al., 2015), polynyas are also recognized as regions harboring the highest densities of upper trophic level organisms in the Southern Ocean (Karnovsky et al., 2007).

Marinov et al. (2006) identified a biogeochemical divide in the Southern Ocean, where waters with a surface potential density of 27.3 kg/m^3 outcrop near the Antarctic divergence. North of the divide, Antarctic Circumpolar Current waters travel north because of Ekman transport driven by strong westerly winds. Surface nutrient drawdown in these Antarctic Circumpolar Current waters decreases the nutrient concentrations in the mode and intermediate waters that subduct in the region of the polar and sub-Antarctic fronts. Therefore, increased high-latitude drawdown of nutrients can lower productivity where mode and intermediate waters resurface at lower latitudes (Marinov et al., 2006). In other words, according to Marinov et al. (2006), increasing surface nutrient drawdown north of the divide has little net impact on global atmospheric pCO$_2$, because biological carbon sequestration will either happen there or at low latitudes. On the other hand, increasing surface nutrient drawdown south of the divide removes carbon from the surface and sequesters it in the ocean's interior for millennia, with the subduction of Antarctic Bottom Water (AABW), which lowers global atmospheric pCO$_2$ more efficiently (Marinov et al., 2006). Shadwick et al. (2014) suggested that the formation and export of dense shelf water from the Mertz polynya and, by extension, similar polynyas around Antarctica, is an effective mechanism to transfer anthropogenic carbon to the ocean's interior. Given the longer residence time of AABW compared to the North Atlantic Deep Water (1,000 years compared to ~300 years; England, 1995), the contribution of this process to the global ocean CO$_2$ sink could be substantial. This motivates our interest in polynya productivity.

In polynyas, the onset of the spring bloom is primarily limited by surface irradiance, ice cover, and periodic deep mixing due to katabatic winds (Vaillancourt et al., 2003). It is only when the mixed layer (ML) has become stratified that phytoplankton growth can overcome losses (Sambrotto et al., 2003). Phytoplankton growth is subsequently controlled by the major limiting nutrient in the Southern Ocean: iron (Martin et al., 1990; Moore et al., 2013). Sources of iron in polynyas are subglacial rivers (Wright et al., 2012), ice shelves (particularly if marine ice is present; Herraiz-Borreguero et al., 2016), icebergs (Duprat et al., 2016; Raiswell et al., 2008), prolonged contact of Fe-rich sediments with upwelled Circumpolar Deep Water (CDW; Arrigo et al., 2015; de Jong et al., 2012; Measures et al., 2013), melting sea ice (Grotti et al., 2005; Lannuzel et al., 2010), and atmospheric deposition in a few particular places (de Jong et al., 2013). The melting rate of the neighboring ice shelves was identified as the main driver of primary production in 46 coastal polynyas around Antarctica (Arrigo et al., 2015). Because these shelves are rapidly losing mass due to climate change (Paolo et al., 2015), their influence on productivity is of regional and global importance.

The objective of this study is to understand the drivers of the observed differences in phytoplankton biomass and primary productivity between three polynyas in East Antarctica: the Dalton, the Mertz, and the Ninnis polynyas. These areas were explored in late December to early January 2016–2017, at the peak of the growing season.

2. Materials and Methods

The R/V *Aurora Australis* sailed to the Dalton polynya (near the Moscow University Ice Shelf), the Mertz polynya (facing the Mertz Glacier Tongue), and the Ninnis polynya (in front of the Ninnis Glacier) between 8 December 2016 and 21 January 2017 (Figure 1a). In the Dalton polynya, conductivity, temperature, and depth (CTD) rosette casts were distributed around margins demarcated by the Moscow University Ice Shelf to the south, the Dalton Iceberg Tongue to the east, 50 km of thick first-year pack ice to the north, and former land-fast sea ice to the west (Figure 1b). Observations were made in the Dalton polynya between 30 December 2016 and 2 January 2017. The Mertz polynya was surrounded by the Mertz Glacier Tongue to the south, large icebergs (B09B and C-15) that blocked land-fast sea ice from drifting to the west, and a field of icebergs to the east (Figure 1c). The Ninnis polynya was bounded to the west by former land-fast sea ice
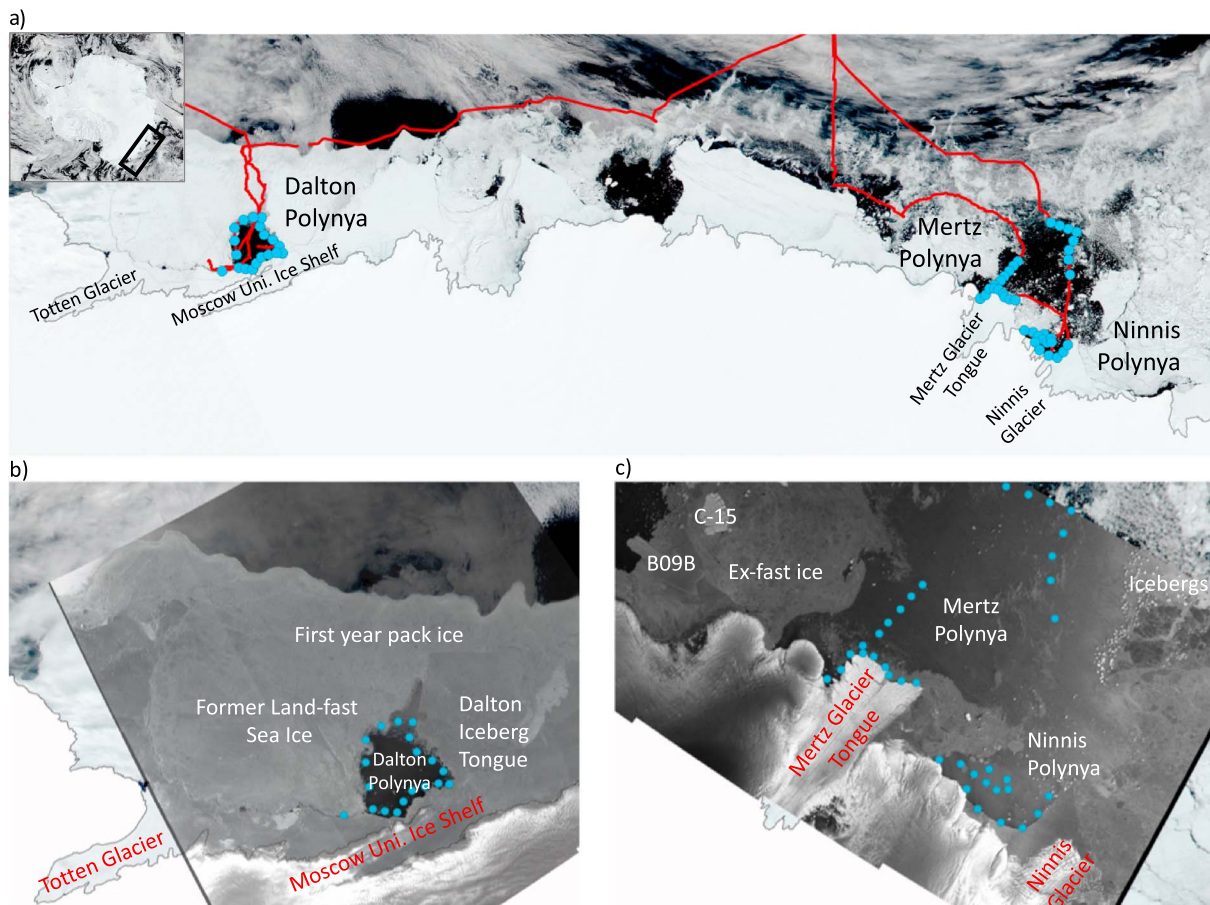
Figure 1. (a) MODIS-Terra visible image of eastern Antarctica, the three polynyas studied (Dalton, Mertz, and Ninnis), the sea ice, and the major glaciers and ice shelves on 4 January 2017 (source: NASA at https://worldview.earthdata.nasa.gov). Sentinel-1b SAR scenes and MODIS-Terra visible images of (b) the Dalton polynya on 4 January 2017 and (c) the Mertz and Ninnis polynyas on 10 January 2017 (provided by PolarView: http://www.polarview.aq/antarctic for SAR scenes and the NASA for MODIS-Terra). Several geographical features are indicated: the Totten Ice Shelf, the Moscow University Ice Shelf, the Mertz Glacier Tongue, the Ninnis Glacier, named icebergs, sea ice, and polynyas. Blue dots indicate CTD locations.

and the Mertz Glacier Tongue, to the south by the coast, and to the east by the Ninnis Glacier and land-fast sea ice (Figure 1c). The Mertz and Ninnis polynyas were studied between 9 and 13 January 2017.

2.1. Sea Surface Parameters

Surface seawater was obtained from the main underway system on board R/V *Aurora Australis*. The seawater intake was located 6.3 m below sea level. Sea surface temperature and salinity were measured every 5 s using a water temperature probe (SBE-38, Sea-Bird Inc., Bellevue, USA) and a thermo-salinograph (SBE-21 TSG, Sea-Bird Inc., Bellevue, USA), respectively. Fluorescence of the underway seawater was measured with a WETStar fluorometer (WS3S-443P, Wetlabs, Sea-Bird Inc., Bellevue, USA).

Sea surface chlorophyll a (Chl a) was measured from the underway system on 44 occasions. Sea water samples of 525 mL were filtered onto 25-mm GF/F filters, extracted in 90% acetone, and stored in the dark at -20 °C for 24–48 h before analysis (Holm-Hansen et al., 1965; Lorenzen, 1966). Chlorophyll a was then measured with a Turner Trilogy fluorometer that had been calibrated with Chl a standards from Turner Designs (Sunnyvale, CA). Surface seawater fluorescence and Chl a correlated significantly ($r^2 = 0.90$, $p < 0.01$; Figure 2a). Therefore, we calibrated the underway fluorescence with the measured sea surface Chl a. It is possible that nonphotochemical quenching at the sea surface under high irradiance periods led to a small underestimation of the sea surface Chl a (Buschmann, 1999; Kaufman et al., 2014). However, given the strong differences in phytoplankton biomass we report in the present study, we believe that nonphotochemical quenching would not have changed the main results of this study.
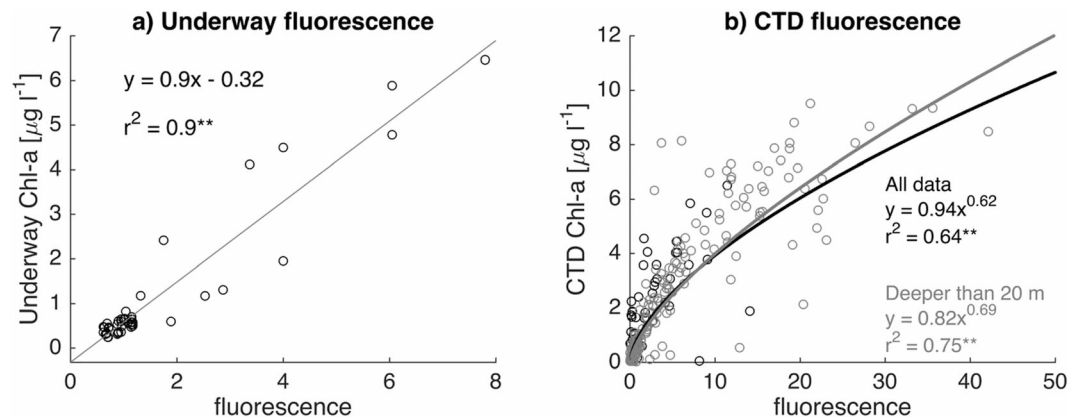
Figure 2. (a) Linear regression between the chlorophyll a concentration (Chl a; μg/L, $N = 44$) measured from underway samples and the corresponding underway fluorescence and (b) power relationship between discrete Chl a concentration (μg/L, $N = 225$) measured from Niskin bottles during CTD casts and the CTD fluorescence at the corresponding depth. Relationships are reported for both all the Chl a measurements and the Chl a measurements below 20 m. Correlation coefficients and significance levels are indicated.

The ratio of dissolved oxygen and argon (O_2/Ar) from the surface seawater intake was measured using a Pfeifer QMS200 quadrupole mass spectrometer and equilibrator inlet (Cassar et al., 2009). The $\Delta(O_2/Ar)$ can be used to determine the net community production (NCP = gross primary production minus community respiration) of O_2, as argon is an inert gas with a solubility similar to O_2 (Cassar et al., 2009). By assuming steady state and neglecting vertical mixing, NCP can be estimated as

$$NCP = k_{O_2} O_{2,sat} \Delta(O_2/Ar) \qquad (1)$$

where k_{O2} is the gas exchange velocity for oxygen, $O_{2,sat}$ is the dissolved O_2 concentration at saturation, and $\Delta(O_2/Ar)$ is the biologically mediated change in O_2. To compute k_{O2}, we used daily 10-m wind speed from the National Centers for Environmental Prediction/National Center for Atmospheric Research reanalyses (Kalnay et al., 1996), weighted to account for wind speed history prior to arrival of the ship (Reuer et al., 2007) and the gas exchange velocity parameterization of Wanninkhof (2014) for long-term winds. We used a photosynthetic quotient of 1.4 as in Laws (1991).

There are known limitations to the use of $\Delta(O_2/Ar)$ to infer NCP, including the assumption of steady state and that vertical mixing is neglected (Shadwick et al., 2017). The upwelling of O_2-poor waters would lead to underestimate NCP via the $\Delta(O_2/Ar)$ method (Cassar et al., 2014). We discuss the implications of these limitations at the end of the results section where NCP rates are presented.

2.2. CTD Profiles

Temperature and salinity profiles were measured using a CTD (Sea-Bird 704, Sea-Bird Inc., Bellevue, USA) with dual conductivity and temperature sensors mounted on the CTD rosette (Rosenberg & Rintoul, 2017). The CTD rosette was also equipped with a fluorometer (ECO-AFL/FL 756, Wetlabs, USA) and a photosynthetic available radiation sensor (QCP2300HP 70110, Biospherical Instruments, San Diego, USA). From the CTD profiles, the depth of the euphotic zone (Zeu) was calculated as the depth at which photosynthetic available radiation reached 1% of surface values (Kirk, 1994). We calculated the depth of the mixed layer as the depth at which the maximum value of the Brunt-Väisälä frequency (N^2) was observed (Karstensen et al., 2017). This method is described as the most ecologically relevant to study phytoplankton vertical distribution in coastal Antarctic waters by Carvalho et al. (2017). However, there were five deeply mixed CTDs in the Dalton polynya for which the maximum N^2 value was found very close to the seafloor and deeper than 250 m. For these CTDs, we estimated the depth of the mixed layer as the depth of the second or third highest N^2 values based on visual estimates.

Samples were collected for salinity, nutrients, Chl a, and photosynthetic parameters. Bottle salinity was determined onboard by conductivity measured with the Guildline Autosal, with a precision of ±0.002 g/

kg. Nitrate and nitrite (NO_x), silicic acid, phosphate, and ammonium concentrations were determined four months postcruise at the CSIRO laboratory (Hobart, Australia) with a Seal AA3 segmented flow instrument following the methods of Wood et al. (1967), Armstrong et al. (1967), Murphy and Riley (1962), and Kérouel and Aminot (1997), respectively (Rees et al., 2019). Samples had been frozen at −20 °C for NO_x, phosphate, and ammonia and refrigerated for silicic acid, which may have induced errors. The precision for reactive NO_x was ±0.02 μM; for reactive phosphate, ±0.02 μM; and for reactive silicic acid, ±0.2 μM. Nutrient concentrations from previous cruises in the Dalton and the Mertz polynyas are also reported in this study with similar measurement precision (Rosenberg & Rintoul, 2010, 2011, 2012, 2016).

Samples for Chl a were collected at five to six discrete depths from the surface down to 200 m. Samples were filtered, extracted, and measured as described previously for sea surface Chl a samples from the underway system. Fluorescence from the CTD and bottle Chl a concentration correlated significantly (both for all the measurements and the measurements below 20 m only, $r^2 = 0.64$ and $r^2 = 0.75$, $p < 0.01$, respectively; Figure 2b). Therefore, we calibrated the CTD fluorescence with the measured bottle Chl a concentrations to obtain full depth profiles for Chl a. As for the underway samples, nonphotochemical quenching may have led to an underestimation of the near-surface Chl a concentration estimated from the CTD fluorescence profile (Buschmann, 1999; Kaufman et al., 2014). In the Ninnis polynya, the fluorescence in the upper 20 m was slightly higher during the low-irradiance period (8 PM to 6 AM) than during the high-irradiance period (6 AM to 8 PM), but within the range of the standard deviation (data not shown). Nonphotochemical quenching was not observed in the Mertz and the Dalton polynyas. Therefore, we believe that nonphotochemical quenching did not affect the main results of this study, that is, the strong biomass differences observed between the three polynyas. Nonetheless, to minimize the possible effect of nonphotochemical quenching, we used the relationship derived from the measurements below 20-m depth.

Photosynthetic parameters such as F_v/F_m, the maximum quantum yield of photosystem II, were measured on 20-mL dark adapted (4 °C in the dark for 30 min) water samples using a pulse-amplitude modulated fluorometer (Water-PAM, Waltz, Effenberg, Germany). Before analyzing daily batch of samples, an Ultra High Purity (Milli-Q) water blank was read. Vials were rinsed 3 times with Milli-Q water between samples to prevent any cross contamination. Sides of the vials were wiped with KimWipes to ensure that no water droplets or fingerprints were left on the glass before analysis.

The ratio of stable oxygen isotopes in seawater ($\delta^{18}O$) was extracted from water samples collected at several depths in the Mertz and Ninnis polynyas. To extend the analysis to the Dalton polynya, $\delta^{18}O$ measurements from the Dalton and the Mertz polynyas from a previous cruise (2014–2015) are used (Aoki et al., 2017; Silvano et al., 2018). From this previous cruise, only the CTD stations that were the closest to the present cruise's CTDs are used, that is, no farther than 50 km. In 2014–2015, the $\delta^{18}O$ measurements were performed with a Finnigan DELTAplus mass spectrometer at the Institute of Low Temperature Science, Hokkaido University, Japan. The measurements precision of the duplicate samples was 0.02‰. In 2016–2017, the $\delta^{18}O$ measurements were performed with a VG Isogas SIRA dual-inlet mass spectrometer at the Central Science Laboratory, University of Tasmania, Australia. The measurement precision of the duplicate samples was < 0.05‰. The fractions of sea ice melt and meteoric water (which originates from direct precipitation into the ocean or the melting of glacial ice: icebergs and ice shelves) were determined from oxygen isotopes and salinity following (Meredith et al., 2008) and Silvano et al. (2018).

We justify the use of $\delta^{18}O_2$ isotopes from a previous cruise as it took place at the exact same time of the year (i.e., late December 2014 to early January 2015) and in the same areas of the Dalton and Mertz polynyas (Aoki et al., 2017; Silvano et al., 2018). Furthermore, potential temperature versus salinity (Θ-S) diagrams of the CTDs in the Dalton and the Mertz polynyas during both the 2014–2015 and the 2016–2017 cruises show that oceanographic conditions were very similar between the two cruises (Figure A1 in Appendix A). In addition, the sea ice melt and meteoric water fractions in the Mertz polynya were very similar between the 2014–2015 and 2016–2017 cruises as explained in section 4 below. Therefore, we consider that the sea ice melt and meteoric water fractions estimated in 2014–2015 represent well the 2016–2017 conditions at this time of the year. Furthermore, various water masses were identified from the Θ-S diagrams, such as Ice Shelf Water (ISW) which was defined as water with potential temperature lower than that of the freezing point at 50 dbar and modified CDW (mCDW) as water with salinity higher than 34.6 g/kg and potential temperature above −1.5 °C (Aoki et al., 2017).

2.3. Satellite Data

Sea surface Chl a was derived from the Sea-Viewing Wide Field-of-View Sensor and the Moderate Resolution Imaging Spectrometer aboard NASA's Aqua satellite. We used the 9-km level-3 seasonal (i.e., austral summer) and eight-day composite images of sea surface Chl a for the period 1997–2017 obtained from the ocean color data distribution site: http://oceandata.sci.gsfc.nasa.gov/.

Daily sea ice concentration from 1997 to 2017 was estimated from the NASA's Nimbus-7 Scanning Multichannel Microwave Radiometer (SMMR) and Defense Meteorological Satellite Program (DMSP)-F13, -F17, and -F18 Special Sensor Microwave/Imager (SSM/I), obtained from the National Snow and Ice Data Centre, University of Colorado in Boulder, CO (http://nsidc.org), as processed using the NASA team algorithms (Cavalieri et al., 2008) with a spatial resolution of 25 km.

3. Results

In the following section, we detail the main physical and biological features of the Mertz, Ninnis, and Dalton polynyas. We show that the phytoplankton biomass and NCP were significantly higher in the Mertz and Ninnis polynyas than in the Dalton polynya.

3.1. Physical Properties

The center of the Dalton polynya was relatively warm with sea surface temperature ranging from 0.0 to 1.5 °C. Sea surface temperature was lower (−1.0 °C) on the edges of the polynya, close to sea ice in the northern and western parts of the polynya, and next to the Moscow University Ice Shelf in the southeast corner of the polynya (Figure 3a). Sea surface salinity was elevated throughout the Dalton polynya (34.0 to 34.5 g/kg) but lower on the edges (between 32.0 and 33.5 g/kg), in particular close to sea ice in the northern and southwestern parts of the polynya (Figure 3b).

Sea surface temperature was generally relatively high throughout the Mertz and Ninnis polynyas, ranging from 0.0 to 1.5 °C (Figure 4a). Sea surface temperature was lower than 0.0 °C southeast of the Ninnis polynya close to land-fast sea ice and northwest of the Mertz polynya. Sea surface salinity was lower in both the Mertz (ranging from 32.5 to 33.5 g/kg; Figure 4b) and the Ninnis (~34.0; Figure 4b) polynyas than in the Dalton polynya (34.0 to 34.3 g/kg; Figure 3b). This lower sea surface salinity may indicate that the Mertz and Ninnis polynyas experienced more sea ice melting than the Dalton polynya. Below 50 m, salinity was lower in the Dalton polynya (34.3 to 34.6 g/kg) than in the Mertz and Ninnis polynyas (34.5 to 35.0 g/kg), probably indicating that the Mertz and Ninnis polynyas had also seen more sea ice formation, and therefore brine formation, in the previous winter.

3.2. Phytoplankton Biomass

Sea surface Chl a was very high in the Dalton polynya (up to 15 μg/L), particularly in the south and east (Figure 3c). In the Mertz and the Ninnis polynyas, sea surface Chl a was lower than in the Dalton, with maximum surface values of ~8 μg/L. There, the highest Chl a patches were observed near the Mertz Glacier Tongue and southeast of the Ninnis polynya (Figure 4c).

In the Dalton polynya, Chl a was lower in the northern transect (Dalton 1; Figure 5b) than in the southern transect (Dalton 2; Figure 5c). In the northern transect, Chl a was low throughout the water column in the northwest and north of the polynya and high in the northeast (up to 2.0 μg/L; Figure 5b). In the northeast and east, Chl a was distributed homogeneously from the surface down to ~150-m depth. This corresponded to where the polynya was deeply mixed, with a ML as deep as 150–200 m in that part of the polynya (Figure 5b). Along the southernmost boundary of the Dalton polynya, Chl a was relatively high (up to 4.9 μg/L) from the surface to ~50- to 80-m depth (Figure 5c), except in the southeast of the polynya where the water column was deeply mixed and Chl a was lower (up to 2.5 μg/L).

In the Mertz and Ninnis polynyas, maximum Chl a was consistently found in a subsurface maximum layer between 20- and 70-m depth (Figure 6). The water column was strongly stratified in both polynyas (Figures 6b–6f), which likely facilitated this distribution. Since Chl a concentration was very high in the subsurface layer of the Mertz and Ninnis polynyas (up to 9.8 and 11.2 μg/L, respectively), the integrated Chl a stocks from the surface to 200-m depth were significantly higher (ANOVA F value = 40.54, $N = 59$, $p < 0.00001$) in the Mertz and Ninnis polynyas (158 to 507 and 152 to 453 mg Chl a/m^2, respectively;
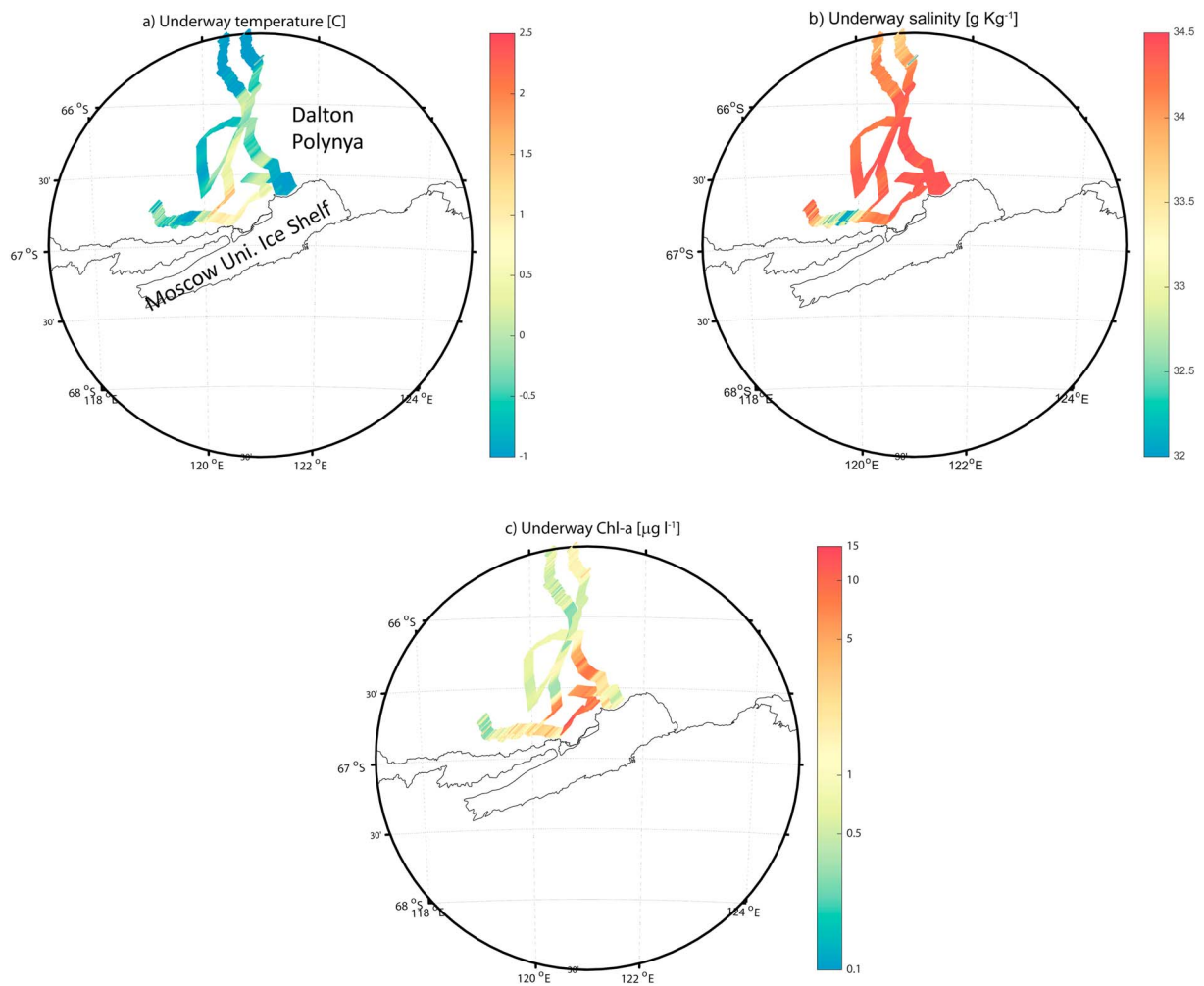
Figure 3. Sea surface (a) temperature (SST; °C), (b) salinity (g/kg), and (c) Chl a concentration (µg/L) measured from the underway system along the ship's route in the Dalton polynya.

Figure 7b) than in the Dalton polynya (9 to 304 mg Chl a/m^2; Figure 7a). The average chlorophyll integrated to 200 m for the Mertz, Ninnis, and Dalton polynyas was 322, 354, and 122 mg Chl a/m^2, respectively.

3.3. Photosynthetic Parameters

In all three polynyas, the maximum quantum yield of photosystem II (F_v/F_m) was below the theoretical optimum of 0.65 for phytoplankton growth (Schreiber, 2004; Figure 8). In the Dalton polynya, the maximum values of F_v/F_m ranged from 0.42 to 0.60 from the southwest to the northeast of the polynya (Figure 8a). F_v/F_m was lower in the north and northwest, 0.12 to 0.32. In the Mertz polynya, the maximum values of F_v/F_m ranged from 0.37 to 0.53 (Figure 8b). In the Ninnis polynya, the maximum values of F_v/F_m were slightly higher than in the Mertz polynya, ranging from 0.42 to 0.55 (Figure 8b). In general, the maximum yield of photosystem II at the depth of the chlorophyll maximum was not significantly different between all three polynyas: 0.39 ± 0.18 for the Dalton polynya, 0.40 ± 0.07 for the Mertz polynya, and 0.44 ± 0.11 for the Ninnis polynya (ANOVA F value = 1.02, N = 69, p = 0.37).

3.4. Primary Productivity

The distribution of surface $\Delta(O_2/Ar)$ was consistent with the distribution of the phytoplankton biomass (Figures 7 and 9). It indicated both biological undersaturation and supersaturation (−8 to +8%) in the Dalton polynya (Figure 9a) with net autotrophy occurring along the coast and the Moscow University Ice Shelf (Figure 9c). In the north of the polynya, a combination of low biomass and heterotrophic respiration

Figure 4. Sea surface (a) temperature (SST; °C), (b) salinity (g/kg), and (c) Chl a concentration (µg/L) measured from the underway system along the ship's route in the Mertz and Ninnis polynyas.
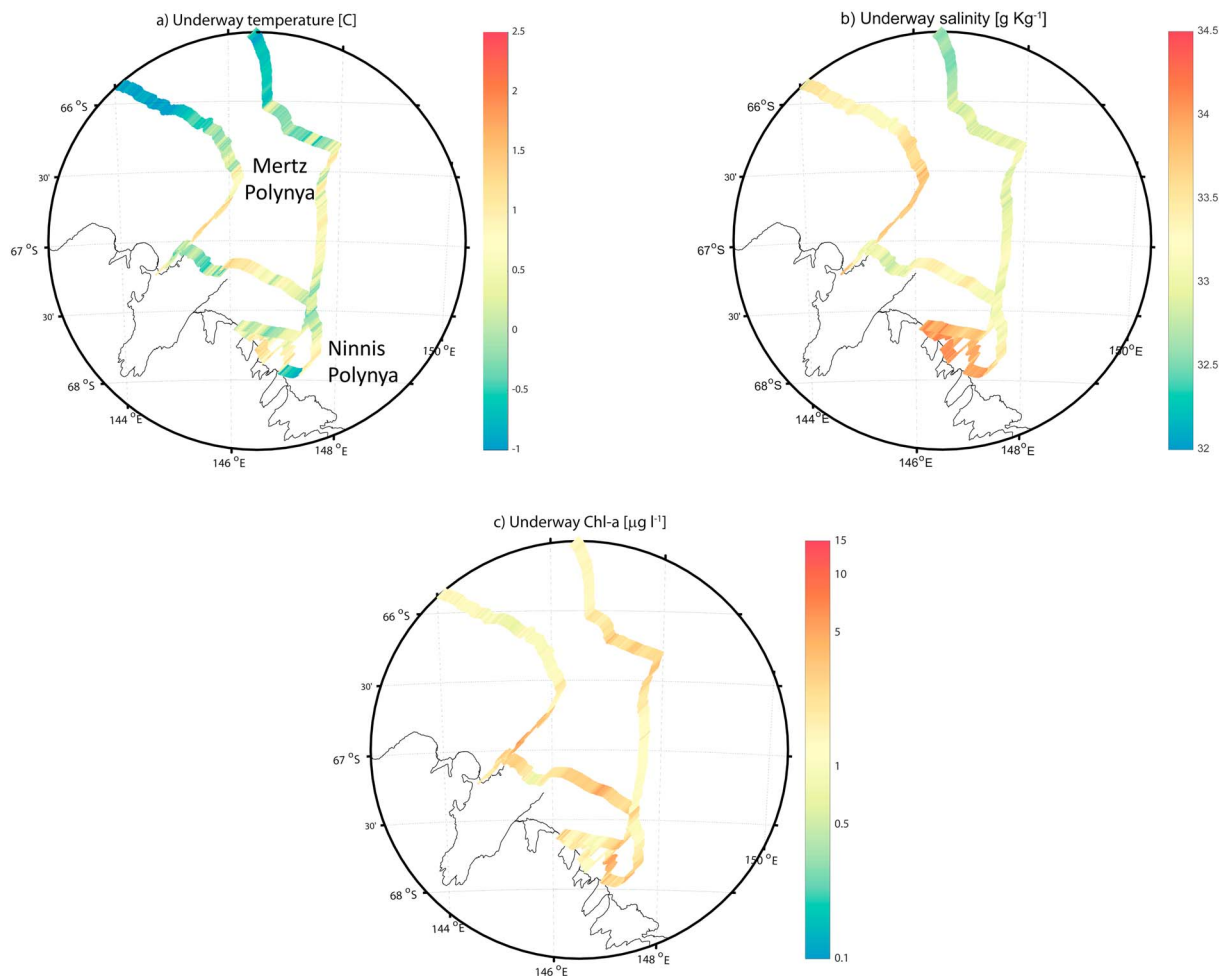
led to a negative $\Delta(O_2/Ar)$, while the water column was strongly stratified (Figure 5b). In the southeast of the polynya, vertical mixing of the water column led to a negative $\Delta(O_2/Ar)$ (Figure 9a and see below). As a result, in the Dalton polynya, there was a large range of NCP values, from −60 to +75 mmol C m^{-2} d^{-1} (Figure 9c).

In contrast, the Mertz and Ninnis polynyas showed strong biological supersaturation of the O_2/Ar ratio (between 5 and 12%; Figure 9b), suggesting that these two polynyas were net autotrophic (Figure 9d). The NCP estimated for the Mertz and Ninnis polynyas was less variable (10 to 60 mmol C m^{-2} d^{-1}; Figure 9d) than in the Dalton polynya. As a result, $\Delta(O_2/Ar)$ was significantly higher in the Mertz and Ninnis (average of 7.2 ± 3.1%) than in the Dalton polynya (average of −0.4 ± 4.5%, ANOVA F value = 3,904, N = 4,020, $p < 0.0001$). As discussed in section 2, in high latitudes, neglecting vertical mixing may lead to the underestimation of NCP via the $\Delta(O_2/Ar)$ method. In the present study, given the shallow ML we observed in the Mertz and Ninnis polynyas (Figure 6) and some parts of the Dalton polynya (Figure 5), the entrainment of O_2-poor waters from deeper layers was unlikely. The only exception is for the southeast of the Dalton polynya where the water column was completely mixed (Figure 5). This could explain the strong O_2/Ar biological undersaturation (Figure 9a), whereas phytoplankton biomass was relatively high in that part of the polynya (up to 2.5 µg/L; Figure 5b). Therefore, NCP estimates derived from $\Delta(O_2/Ar)$ in that area were likely underestimated.

In comparison, the NCP prior to sampling was assessed through the drawdown of nitrate and phosphate in the upper 200 m (Figures 7c and 7d), following Moreau et al. (2013). For this, the deep (200 m) nitrate and
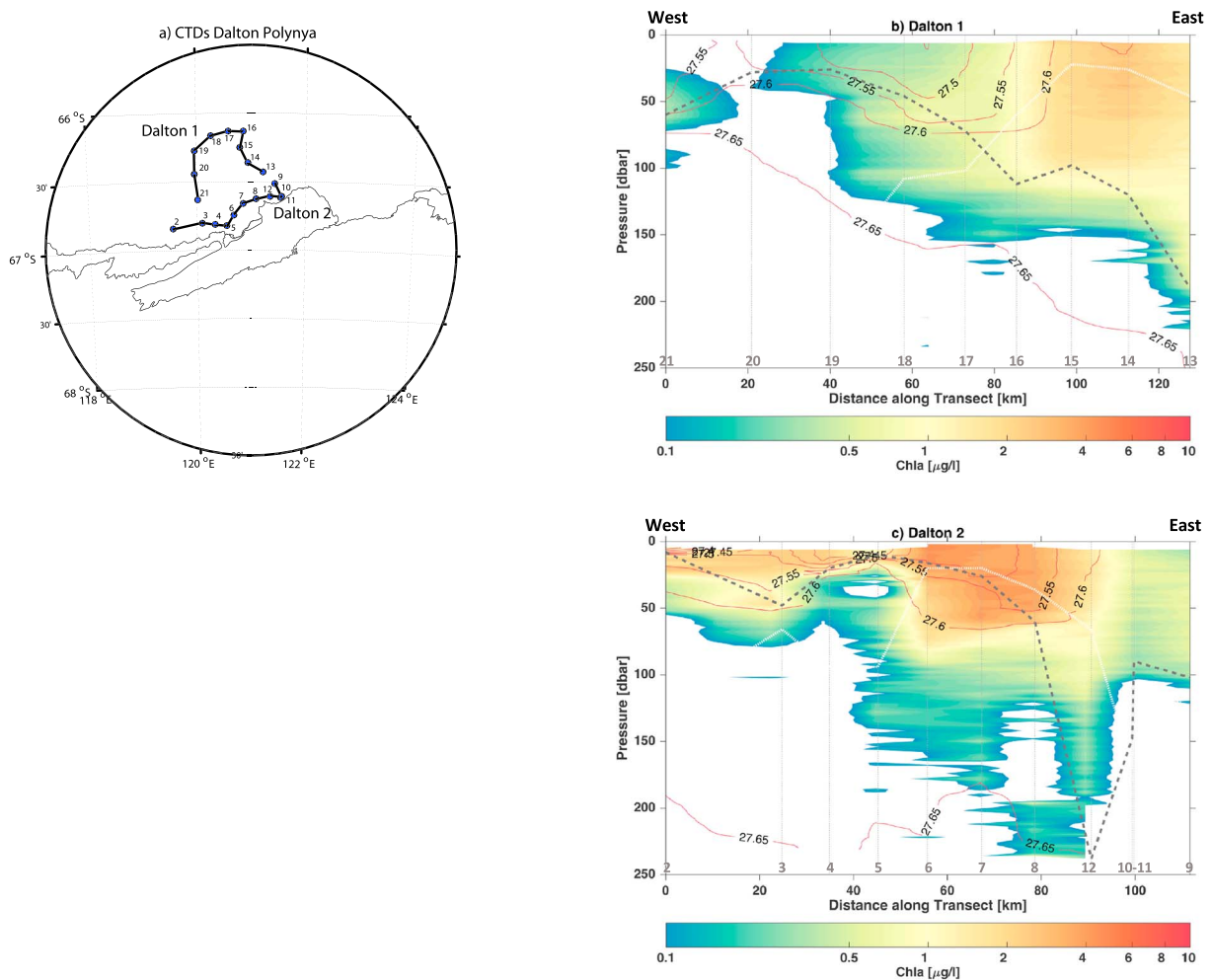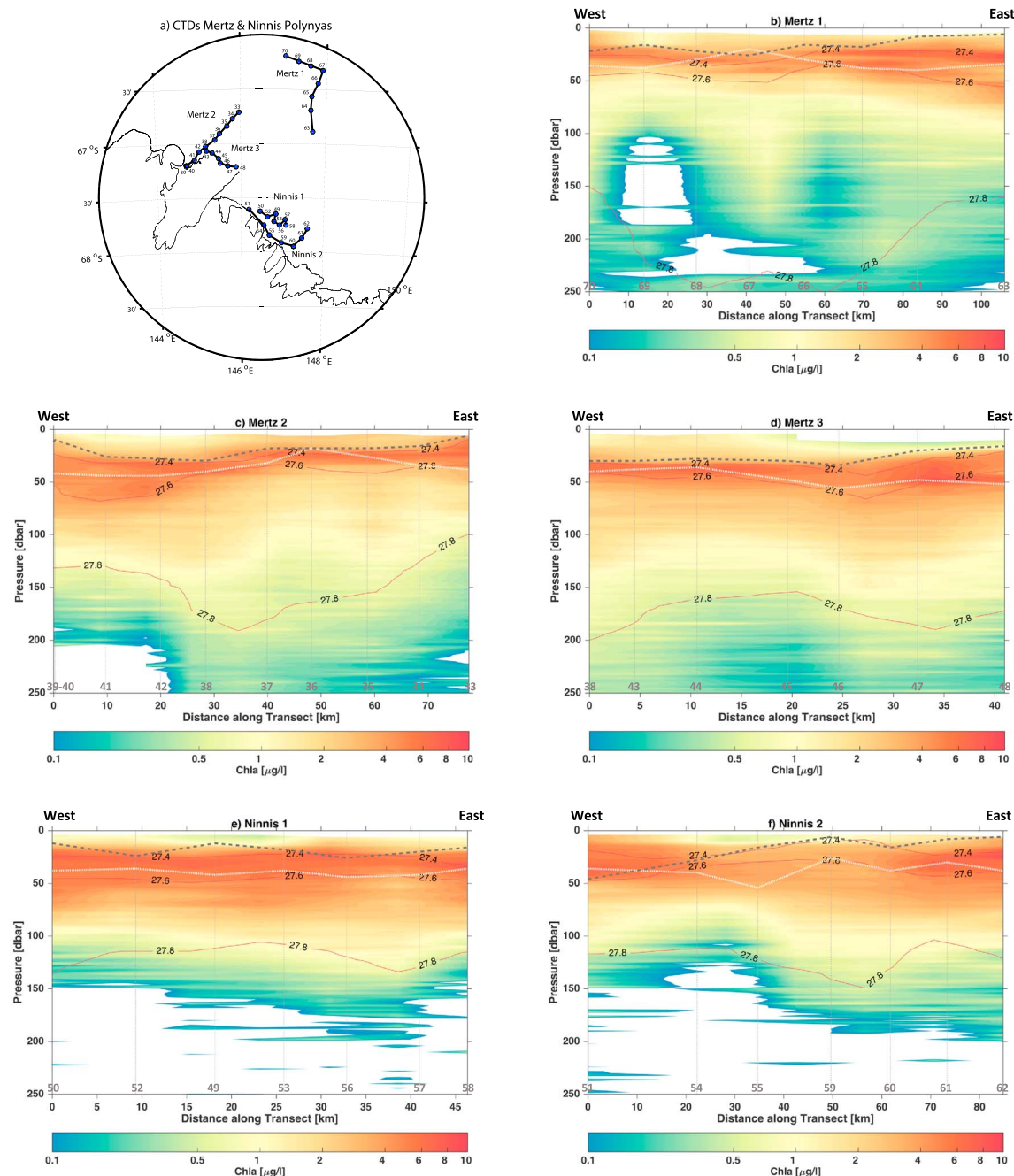
Figure 5. (a) West-east CTD transects across the Dalton polynya. Chl *a* concentration (µg/L) for the west-east transects: (b) Dalton 1 and (c) Dalton 2. The following features are indicated: potential density isopycnals (σ_Θ; dark red), the depth of the mixed layer (ML; dashed gray line), and the depth of the euphotic zone (Zeu; dotted white line). Because of various cruise imperatives, the track of the ship in Figure 3 is different. The transects were chosen here to give a two-dimensional view of the Dalton polynya. The CTD numbers are indicated in gray in (b) and (c).

phosphate values were considered as representative of winter concentrations in surface waters before the onset of the production season (early November); the nutrient drawdown was transformed to carbon units following Redfield et al. (1963). The observed nitrate and phosphate concentrations in the upper 200 m in the three polynyas are presented in Figure A2 in Appendix A. Phosphate-derived integrated NCP was significantly correlated with that retrieved from nitrate drawdown ($r^2 = 0.87$, $N = 55$, $p < 0.01$). Throughout the rest of the manuscript, we use the integrated NCP derived from nitrate drawdown (Figures 7c and 7d). Results are consistent with the distribution of the integrated phytoplankton biomass. That is, NCP was significantly higher in the Mertz and Ninnis polynyas (2.6 to 8.9 and 3.0 to 5.7 mol C/m^2, respectively; Figure 7d) than in the Dalton polynya (0.3 to 4.7 mol C/m^2; Figure 7c; ANOVA F value = 25.16, $N = 55$, $p < 0.01$). Results are also consistent with the distribution of the NCP estimates derived from $\Delta(O_2/Ar)$ even though they represent the mixed layer NCP integrated on a much longer time scale, that is, from the start of the growing season.

Finally, to understand the main drivers of primary productivity in the three polynyas, we ran nonparametric Spearman rank-order correlations between the NCP derived from nitrate drawdown in the mixed layer, the Chl *a* integrated in the upper 200 m, and the various physical properties encountered in the polynyas. These results are presented in Table 1 and discussed throughout section 4.

Figure 6. (a) West-east CTD transects across the Mertz and the Ninnis polynyas. Chl *a* concentration (µg/L^1) for the west-east transects: (b) Mertz 1, (c) Mertz 2, (d) Mertz 3, (e) Ninnis 1, and (f) Ninnis 2. The following features are indicated: potential density isopycnals (σ_θ; dark red), the depth of the mixed layer (ML; dashed gray line), and the depth of the euphotic zone (Zeu; dotted white line). Because of various cruise imperatives, the track of the ship in Figure 4 is different. The transects were chosen here to give a two-dimensional view of the Mertz and Ninnis polynyas. The CTD numbers are indicated in gray in (b)–(e).

4. Discussion

4.1. Icescape of the Dalton, Mertz, and Ninnis Polynyas

The Totten and Mertz Glaciers are outlet glaciers for the two largest volumes of marine-based ice in East Antarctica, the Aurora Basin and the Wilkes Basin, respectively. Because temperature freezing point decreases by 0.75 °C for every 1,000-m increase in ocean depth, their deep grounding lines (1,500 to
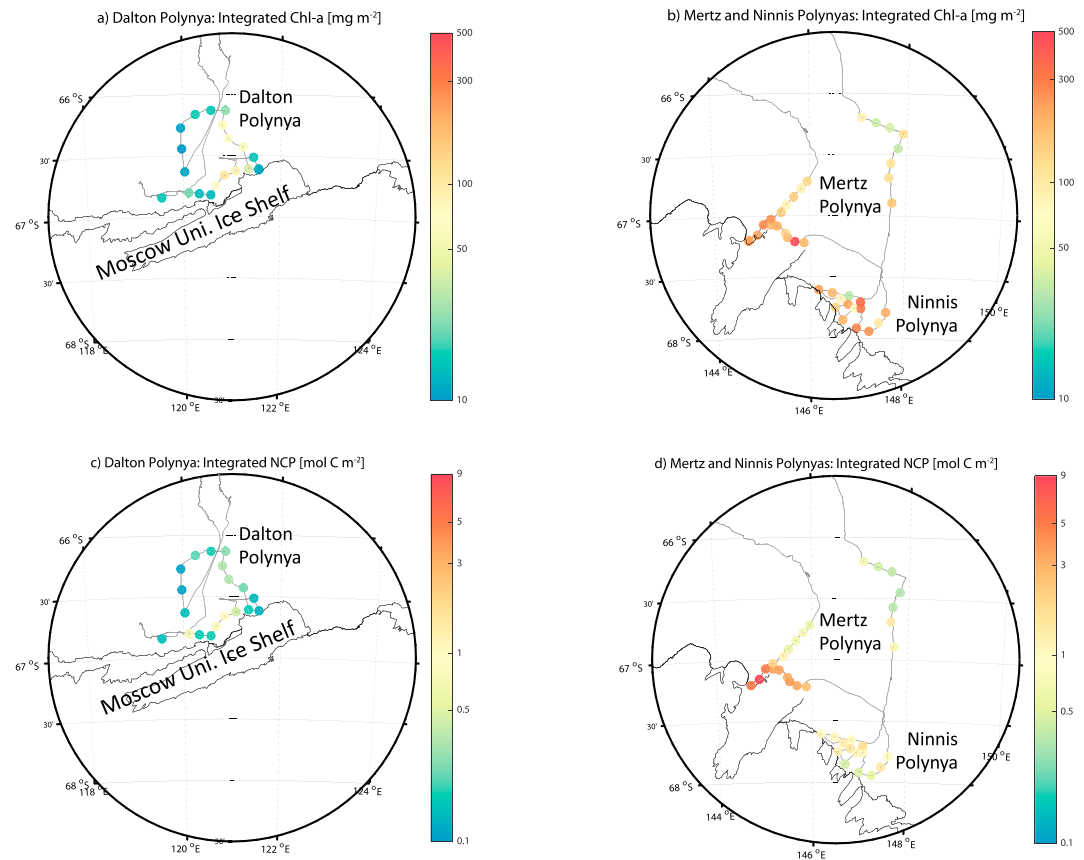
Figure 7. Depth-integrated Chl *a* (mg/m^2) for (a) the Dalton polynya and (b) the Mertz and Ninnis polynyas. Chlorophyll *a* is integrated to a depth of 200 m for ease of comparison. Depth-integrated net community production (NCP; mol C/m^2) prior to the cruise estimated from nitrate drawdown in the upper 200 m for (c) the Dalton polynya and (d) the Mertz and Ninnis polynyas.

2,000 m) make these glaciers particularly sensitive to melting (Rignot & Jacobs, 2002) and potentially large contributors to sea level rise and nutrient supply (Silvano et al., 2016).

No dense shelf water (DSW) formation has been observed in the Dalton polynya (Silvano et al., 2017; Williams et al., 2011). Warm mCDW is widespread on the continental shelf surrounding the Totten Ice Shelf, and is persistently found in the Dalton polynya (Silvano et al., 2017, 2018). The absence of DSW allows
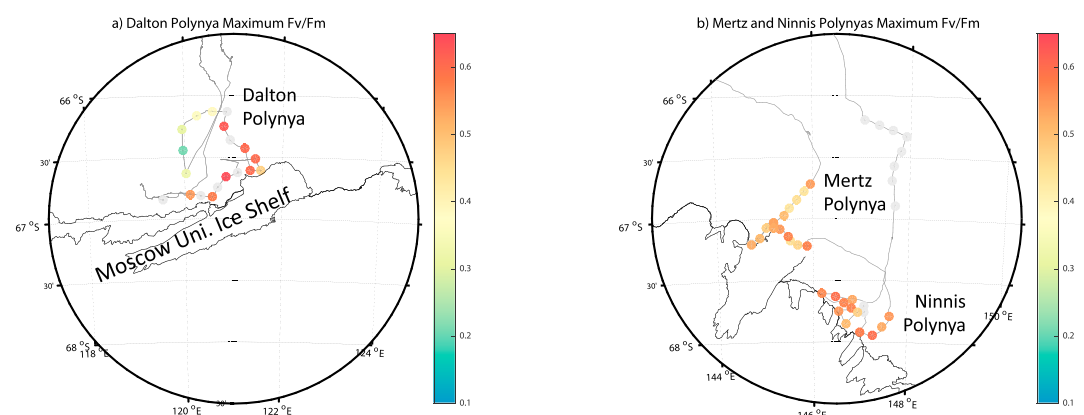
Figure 8. Maximum value of the quantum yield of PSII (F_v/F_m; red dots) in the (a) Dalton polynya and (b) the Mertz and Ninnis polynyas. Light gray CTD profiles indicate the absence of data.
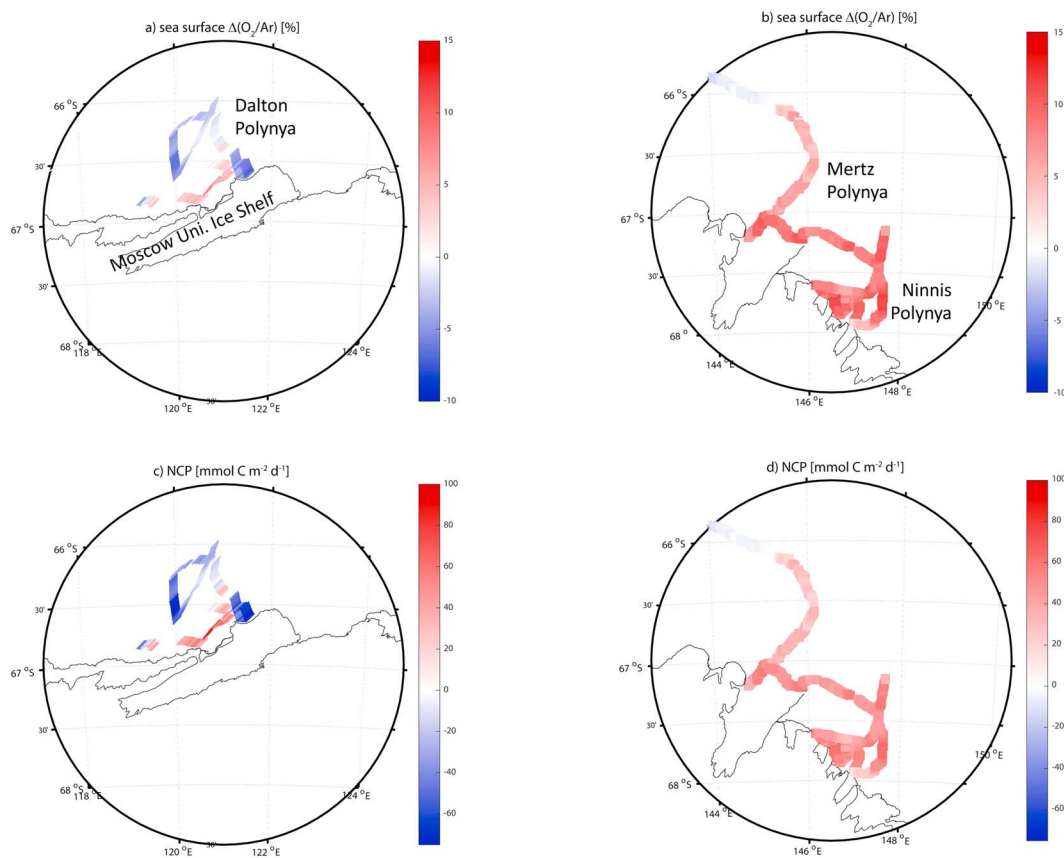
Figure 9. Sea surface $\Delta(O_2/Ar)$ (%) in (a) the Dalton polynya and (b) the Mertz and Ninnis polynyas. Estimated net community production (NCP; mmol C m^{-2} d^{-1}) in (c) the Dalton polynya and (d) the Mertz and Ninnis polynyas.

Table 1

Nonparametric Spearman Rank-Order Correlation Matrix Between the Net Community Production (NCP) Derived From Nitrate Drawdown in the Mixed Layer (mol C/m^2), the Chl a Integrated Down to 200 m (mg/m^2), the Average Salinity in the Top 20 m (g/kg; Sea Surface Salinity), the Average Temperature in the Top 20 m (°C; Sea Surface Temperature), the Depth of the Mixed Layer (ML; m), the Total Meteoric Water Fraction in the Top 500 m (‰), the Minimum Depth at Which the Ice Shelf Water Is Encountered (ISW Depth; m), the Thickness of the ISW Layer (m), the Minimum Depth at Which the Modified Circumpolar Deep Water Is Encountered (mCDW Depth; m), the Thickness of the mCDW Layer (m), and the Total Sea Ice Melt Fraction in the Top 50 m (‰)

	NCP	Chl a	SSS	SST	ML	Meteoric Water	ISW Depth	ISW Layer	mCDW Depth	mCDW Layer	Sea Ice Melt
NCP	1	**0.83**	**−0.68**	0.39	0.21	0.48	0.17	0.12	**−0.88**	−0.22	**0.80**
Chl a		1	**−0.56**	0.36	0.34	0.35	0.26	0.33	**−0.92**	−0.40	**0.68**
SSS			1	−0.15	−0.42	−0.43	−0.26	−0.29	0.23	0.20	**−0.85**
SST				1	0.37	0.08	0.33	0.44	−0.50	−0.05	−0.09
ML					1	0.13	0.33	0.41	**−0.54**	−0.12	0.18
Meteoric water						1	0.33	0.45	0.45	−0.01	0.29
ISW depth							1	**0.95**	NaN	NaN	0.38
ISW layer								1	NaN	NaN	0.38
mCDW depth									1	0.40	**−0.55**
mCDW layer										1	0.03
Sea-ice melt											1

Note. The data used for this correlation matrix are from the 2014–2015 and the 2016–2017 cruises in the Dalton, Mertz, and Ninnis polynyas (see section 2). Significant Spearman rank-order correlation coefficients are shown as bold and underlined if significant with $p < 0.01$ and an absolute coefficient higher than 0.5. NaN values are reported for the correlation between ISW and mCDW layer and depth because these water masses only co-occurred at two CTD stations.

mCDW to fill the bottom layer of the shelf and be transported, through troughs, to the base of the Totten Ice Shelf (Rintoul et al., 2016), where its heat content would melt the base of the ice shelf. This mechanism could explain why the Totten Ice Shelf is melting at very high rates, comparable to West Antarctic ice shelves (Rignot et al., 2013). The neighboring Moscow University Ice Shelf also has comparably high rates of basal melting (Rignot et al., 2013), possibly also under the influence of mCDW (Silvano et al., 2017). The buoyant glacial meltwater from these ice shelves might have a strong influence on the primary productivity of the adjacent coastal waters (e.g., Herraiz-Borreguero et al., 2016), by affecting both the hydrography and the supply of nutrients to the area.

The Mertz and Ninnis polynyas correspond to one of the main four regions where AABW forms, together with the Weddell Sea, the Ross Sea, and Cape Darnley (Ohshima et al., 2016; Rintoul, 1998). In February 2010, the B09B iceberg collided with the Mertz Glacier Tongue, calving a 78 × 40-km giant iceberg, named C28 (Young et al., 2010). Following this event, icebergs, including large sections of B09B, grounded in the Adelie Depression, west of the Mertz Glacier, which strongly modified the entire icescape of the Mertz and Ninnis polynyas. As a consequence, the production of sea ice in the Mertz polynya decreased by ~20% immediately postcalving (Tamura et al., 2012) and by ~40% subsequently (Ohshima et al., 2016), resulting in a significant decrease in AABW production (Snow et al., 2018). In terms of primary productivity, Shadwick et al. (2013, 2017) showed that NCP in the Mertz polynya has doubled postcalving (i.e., 2012 and 2013) compared to precalving (2001 and 2008). These effects are similar to the breakup of the Larsen A Ice Shelf in January 1995, which created new areas of highly productive open water in the Weddell Sea (Bertolin & Schloss, 2009). The breakup of glaciers and ice shelves along the whole Antarctic Peninsula may have increased productivity by up to 3.5 Tg C m^{-2} yr^{-1} (Peck et al., 2010). In the context of this work, the changing icescape of the Mertz and Ninnis compared to the Dalton may have had a significant impact on the productivity of the three polynyas.

4.2. Drivers of Phytoplankton Biomass in Three East Antarctic Polynyas

Despite having similar optimal growing conditions (F_v/F_m; Figure 8), the integrated phytoplankton biomass and nitrate-derived NCP were significantly higher in the Mertz and Ninnis polynyas (158 to 507 and 152 to 453 mg Chl a/m^2 and 2.6 to 8.9 and 3.0 to 5.7 mol C/m^2, respectively; Figures 7b–7d) compared to the Dalton polynya (9 to 304 mg Chl a/m^2 and 0.3 to 4.7 mol C/m^2; Figures 7a–7c). In the following sections, we investigate the main drivers of primary productivity in Antarctic polynyas that could explain the observed differences. To do this we pool the physical, environmental, and biological data from the present (2016–2017) cruise to the Dalton, Mertz, and Ninnis polynyas with the same type of data from a previous (2014–2015) cruise in the Dalton and Mertz polynyas (Aoki et al., 2017; Silvano et al., 2018).

4.2.1. Stratification and Light Penetration

Stratification is usually required to trigger phytoplankton growth in Antarctic polynyas (Arrigo et al., 2003). Overall, the ML depth was significantly and positively correlated with sea surface temperature averaged over the upper 20 m ($r^2 = 0.25$, $N = 58$, $p < 0.01$) in the Dalton, Mertz, and Ninnis polynyas. The water column was strongly stratified in the Mertz and Ninnis polynyas with average ML depths of 20.2 ± 8.1 and 18.1 ± 10.6 m, respectively. The water column was more deeply mixed in the Dalton polynya: the ML depth was 50.0 ± 36.7 m on average, excluding five southeast CTD casts (CTDs 9–13 in Figure 5a). For these five southeast CTD casts, the ML depth ranged between 90 and 200 m. Strong katabatic winds blew from the southeast for 1.5 days when the Dalton polynya was visited, which delayed sampling. Even though it is unlikely that a single storm event could mix the water column down to 200 m, previous southeasterly katabatic wind events and buoyancy forcing may have completely mixed the water column in the southeast corner of the polynya prior to our visit. The austral summer typically experiences lower winds in east Antarctica, although occasional strong katabatic winds can occur in Adelie Land (Massom et al., 1998; Periard & Pettre, 1993) and thoroughly mix the water column. The shallower ML in the Mertz and Ninnis polynyas could have explained the higher phytoplankton biomass observed there. However, no correlations were found between the ML depth and the integrated Chl a or the integrated NCP estimated from nitrate drawdown (Table 1). This suggests that stratification did not drive the contrast in biomass observed in our study.

Note that, even though it did not drive the contrast in biomass in the three polynyas, stratification may have played an important role in phytoplankton physiology. Indeed, the photosynthetic efficiency was lower in the surface waters of the Mertz and the Ninnis polynyas (Figure 8), possibly because high visible and

ultraviolet radiation photoinhibited the growth of phytoplankton (Fritz et al., 2008; Moreau et al., 2015). This could explain the distribution of Chl *a* in the water column (Figures 5 and 6). The depth of the subsurface Chl *a* maximum was similar between the Mertz (31.4 ± 8.6 m), the Ninnis (32.6 ± 10.5 m), and the Dalton (33.5 ± 26.0 m) polynyas, although more variable and less well defined in the latter.

4.2.2. Iron From Glacial Ice

Iron is the main limiting nutrient for primary producers in Antarctic surface waters (Moore et al., 2013; Tagliabue et al., 2017). While low-latitude environments of the Southern Ocean may receive atmospheric inputs of iron, coastal Antarctica generally does not (Heywood et al., 2014), except for places such as McMurdo Sound which is in close proximity to the dry valleys and Mount Erebus volcano (de Jong et al., 2013). The main sources of iron to coastal Antarctica are (1) melting ice shelves, glaciers, and icebergs, particularly if marine ice is present (Herraiz-Borreguero et al., 2016; Lin et al., 2011); (2) upwelled iron-rich mCDW interacting with Fe-rich sediments (de Jong et al., 2012; Measures et al., 2013; Sherrell et al., 2015); and (3) sea ice (Lannuzel, Vancoppenolle, et al., 2016). We examine each of these sources in this and the following two sections.

The influence of melting ice shelves and glaciers on coastal Antarctica's iron pool has been demonstrated in some areas like the Amundsen Sea and Prydz Bay (Gerringa et al., 2012; Herraiz-Borreguero et al., 2016). Gerringa et al. (2012) found that the dominant pool of dissolved iron that fuels the very large phytoplankton blooms in the Amundsen Sea comes from melting at the base of the Pine Island Glacier. Herraiz-Borreguero et al. (2016) suggested that the dissolved and particulate iron from the marine ice present under the Amery Ice Shelf is the primary source of iron that sustains the phytoplankton bloom in Prydz Bay, which is the second most productive bloom in Antarctica, after the Amundsen Sea (Arrigo et al., 2015).

While intrusions of warm mCDW onto some continental shelves of Antarctica accelerate the melting of ice shelves, such as the Pine Island Ice Shelf (Dutrieux et al., 2014), only relatively cold dense shelf water (DSW) reaches the cavities below the Mertz Glacier Tongue and the Ninnis Ice Shelf (Silvano et al., 2016). Following basal melting, newly formed ISW exits the ice shelf cavity at the calving front and is potentially rich in iron (Herraiz-Borreguero et al., 2016). At the Mertz Glacier, this outflow is strongest on the western side of the ice front but relatively deep (>200-m depth; Figure 10b). In the Ninnis polynya, our results indicate the presence of ISW between 250 and 700 m throughout the polynya (Figure 10b). The outflow of glacial meltwater from the Totten Ice Shelf is located on the western side of the calving front (Silvano et al., 2017), and is not likely to directly influence primary productivity in the Dalton polynya. However, the outflow of ISW from the Moscow University Ice Shelf is widespread along the coast and relatively shallow (50- to 100-m depth), south of the Dalton polynya (Figure 10a; Silvano et al., 2017). This area corresponds to where productivity is the highest in the Dalton polynya (Figures 5, 7a, and 7c), suggesting that glacial meltwaters from the Moscow University Ice Shelf may sustain part of the primary productivity in this polynya.

In comparison to the very localized ISW, we observe, as in Silvano et al. (2018), that meteoric water is distributed throughout the water column in the Mertz and the Ninnis polynyas and in the upper 400 m in the Dalton polynya, as a remnant of previous years accumulation (Figure 11a). The origin of meteoric water is either direct precipitation into the ocean or the melting of ice shelves and icebergs and can, as for ISW, be used as a proxy for the presence of glacial meltwater. However, in the present study, neither the integrated phytoplankton biomass nor the NCP derived from nitrate drawdown were correlated to either the meteoric water fraction in the top 500 m, the depth at which ISW was encountered in the water column or the thickness of the ISW water layer (Table 1). Therefore, even though glacial meltwater may have played a localized role in phytoplankton dynamics (e.g., south of the Dalton polynya), this result suggests that glacial meltwater is not the primary driver of the strong differences we observed in the phytoplankton biomass and NCP between the Dalton, Mertz, and Ninnis polynyas. Our findings contrast with recent studies which showed that glacial meltwater is the main driver of primary production in the coastal waters of the Amundsen Sea and the west Antarctic Peninsula (Eveleth, Cassar, Doney, et al., 2017; Sherrell et al., 2015).

4.2.3. Iron From Modified Circumpolar Deep Water

The presence of mCDW has been reported in the Mertz and the Dalton polynyas (Rintoul, 1998; Silvano et al., 2017), indicating that mCDW is a potential source of iron for these coastal ecosystems (Sedwick et al., 2008). In the Mertz polynya, DSW occupies the bottom layer on the shelf, and therefore, the lighter
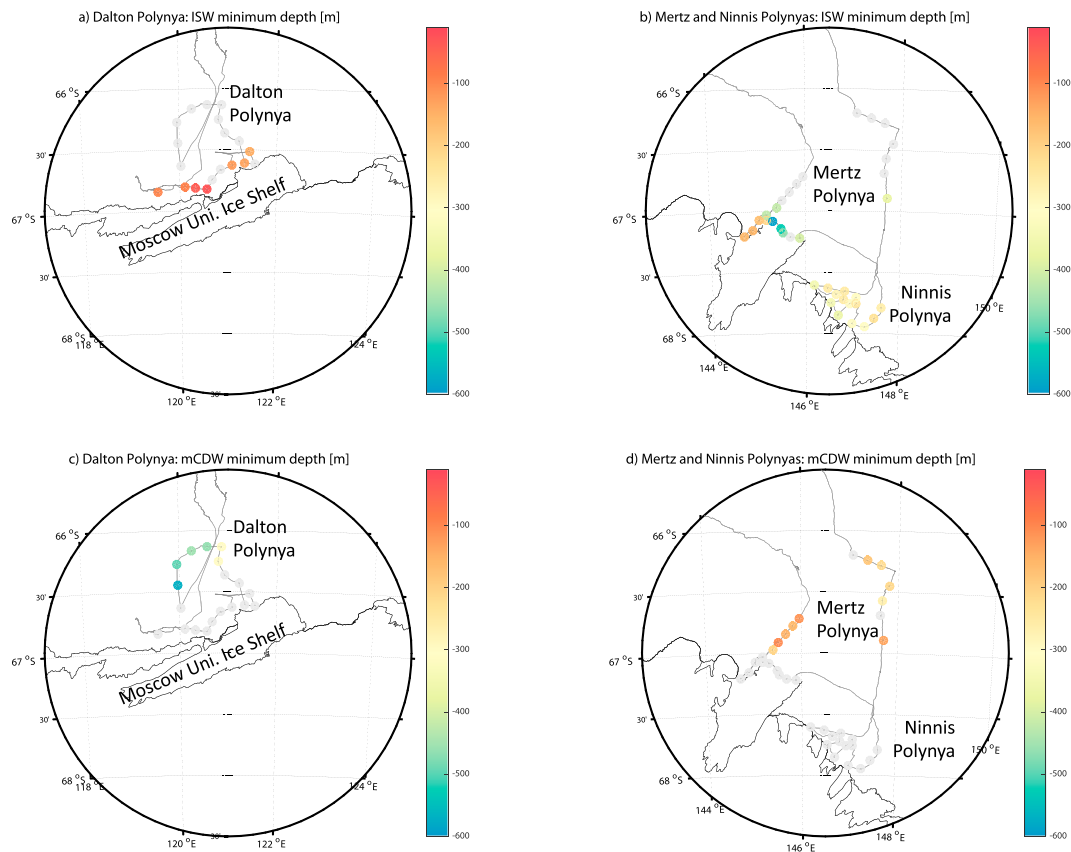
Figure 10. Maps of the minimum depth (m) at which (a and b) ice-shelf water (ISW) and (c and d) modified circumpolar deep water (mCDW) were encountered in the Dalton, Mertz, and Ninnis polynyas during the 2016–2017 campaign. The minimum depths are not presented for the stations where ISW or mCDW was not observed. These CTD stations are indicated by light gray dots.

mCDW is found at shallower depths (between 100 and 350 m), in CTD stations north of the Mertz Glacier Tongue (Figure 10d). In the Ninnis polynya, no mCDW was observed (Figure 10d). In contrast, in the Dalton polynya, where no DSW is formed, the mCDW is the densest water mass on the shelf and occupies the bottom layer of the northern and central part of the polynya, at depths ranging from 300 to 750 m (Figure 10c). This is consistent with previous observations of mCDW in these polynyas (Silvano et al., 2016). We observed that both the integrated phytoplankton biomass and NCP significantly and negatively correlated with the depth at which the mCDW was observed (rho = −0.92, $p < 0.01$ and rho = −0.88, $p < 0.01$, respectively; Table 1 and Figure 11c), implying that the shallower the mCDW layer is, the more productive the water column is. However, as the presence of mCDW is not widespread in the Mertz Polynya and mCDW is not observed in the Ninnis polynya (Figures 10c and 10d), the depth of the mCDW cannot be the sole driver or of the large differences we observed in the phytoplankton biomass and NCP between the three polynyas.

In addition, it is usually assumed that, around Antarctica, the upwelling of CDW on continental shelves through troughs resuspends sediments, a process that increases the iron content of mCDW (de Jong et al., 2012; Measures et al., 2013; Sherrell et al., 2015). In the Dalton polynya, mCDW was in contact with the sediments, which likely increased its iron content. However, given the vertical distribution of water masses in the Dalton polynya, it is unlikely that mCDW mixed with surface waters (Silvano et al., 2018). At Mertz, on the other hand, the mCDW is generally not in contact with sediments on the seafloor.

4.2.4. Iron (and Algae) From Melting Sea Ice

This oceanographic campaign took place in late December to early January, at the peak of the sea ice melting season. Air temperature was between −4 and +3 °C during our visit to the polynyas. In addition, we studied
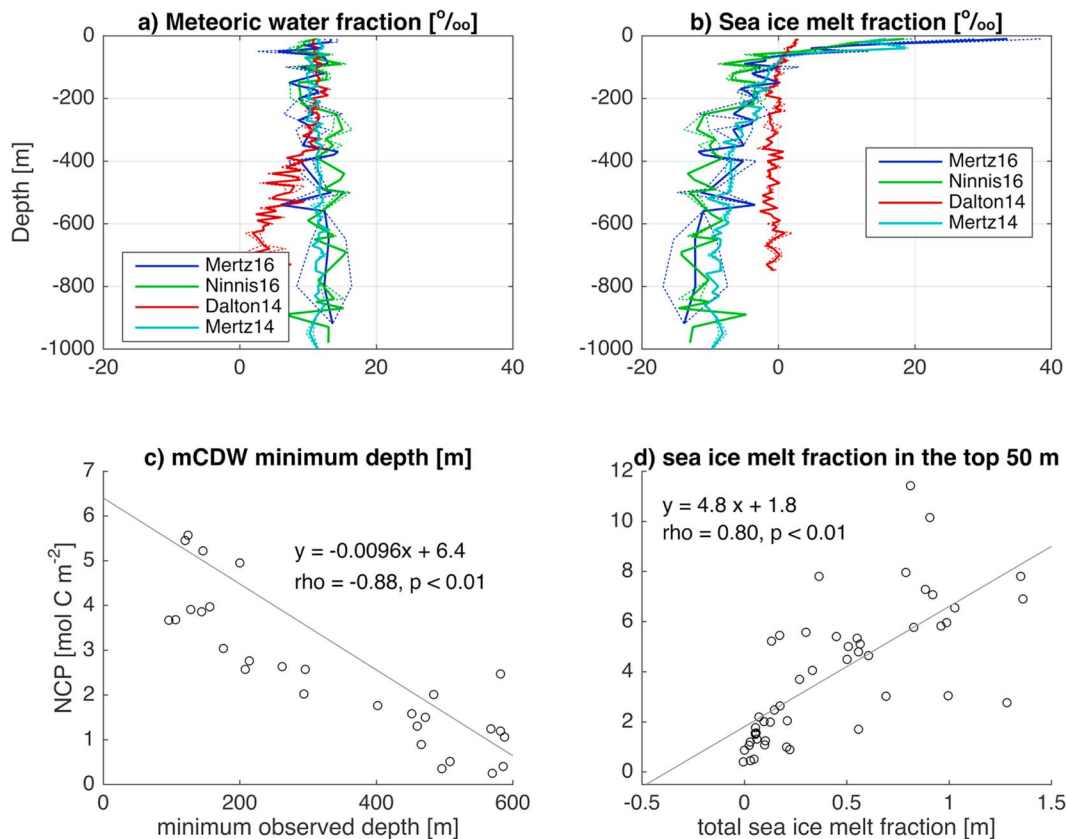
Figure 11. Average (±standard error) fractions of (a) meteoric water (‰) and of (b) sea ice meltwater (‰), determined from salinity and $\delta^{18}O$ measurements in the Dalton, Mertz, and Ninnis polynyas during the 2014–2015 and 2016–2017 campaigns. Net community production (NCP; mol C/m²) estimated from nitrate drawdown in the mixed layer (for the 2014–2015 and the 2016–2017 campaigns) versus (c) the minimum depth at which circumpolar deep water (mCDW) is encountered and (d) the total sea ice meltwater fraction in the top 50 m (m). Results from the Dalton and the Mertz polynyas are plotted in (c) as no mCDW was observed in the Ninnis polynya. Results from the three polynyas (Dalton, Mertz, and Ninnis) are plotted in (d). Linear regressions are indicated.

seven sea ice floes at or near the Dalton, Mertz, and Ninnis polynyas following Lannuzel, Chever, et al. (2016). We could visually assess the extremely advanced stage of sea ice decay, both from ship-based and on-floe observations. We therefore envisage that melting sea ice seeded seawater with iron and algae prior to and during our visit to the polynyas (Lannuzel et al., 2008).

Sea ice melting was likely more intense in the Mertz and Ninnis polynyas than in the Dalton polynya. This is suggested by the sea surface salinity, which was significantly lower in the Mertz and Ninnis polynyas (average of 33.18 ± 0.33 g/kg; Figure 4b) than in the Dalton polynya (average of 34.01 ± 0.33 g/kg; ANOVA F value = 11,794, $N = 11,905$, $p < 0.0001$; Figure 3b). This is confirmed by the sea ice melt fraction which shows both a strong signal of sea ice growth from the previous winter at depth (i.e., negative sea ice meltwater fraction) and a strong signal of seasonal sea ice melt in the top 70 m of the Mertz and Ninnis polynyas (Figure 11b). In comparison, in the Dalton polynya, sea ice growth and melt were much less pronounced (Figure 11b). Moderate Resolution Imaging Spectrometer–Terra visible images suggest that more sea ice drifted across the Mertz and Ninnis polynyas (as can be seen in Figure 1a) than in the Dalton polynya, which was always free of ice from late October 2016 (https://worldview.earthdata.nasa.gov/).

The sea ice meltwater fraction may explain the higher phytoplankton biomass and NCP observed in the Mertz and Ninnis polynyas compared to the Dalton polynya. Indeed, both the integrated phytoplankton biomass and NCP correlated significantly with the sea ice meltwater fraction (rho = 0.68, $p < 0.01$ and rho = 0.80, $p < 0.01$, respectively; Table 1 and Figure 11d). To corroborate the importance of sea ice
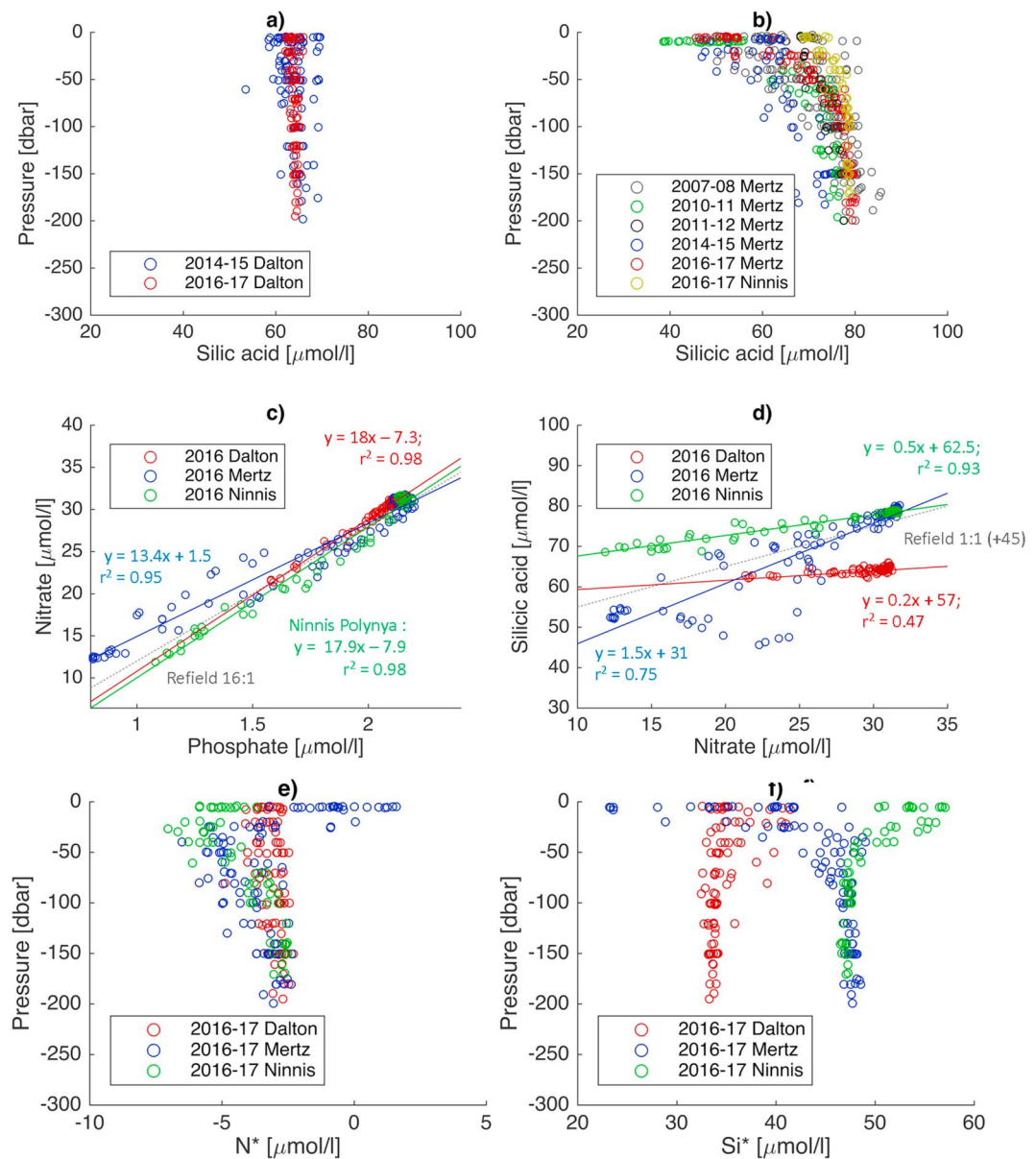
Figure 12. Silicic acid concentration (μmol/L) in (a) the Dalton polynya (2014–2015 and 2016–2017 cruises) and (b) the Mertz (2007–2008, 2010–2011, 2012–2013, 2014–2015, and 2016–2017 cruises) and Ninnis (2016 cruise) polynyas. The sampling station numbers and dates are Dalton 2014–2015 ($N = 81$; 25 December 2014 to 08 January 2015), Dalton 2016–2017 ($N = 20$; 30 December 2016 to 02 January 2017), Mertz 2007–2008 ($N = 37$; 24 December 2007 to 03 January 2008), Mertz 2010–2011 ($N = 25$; 26–29 January 2011), Mertz 2011–2012 ($N = 6$; 10–11 January 2012), Mertz 2014–2015 ($N = 51$; 11–18 January 2015), Mertz 2016–2017 ($N = 23$; 09–13 January 2017), and Ninnis 2016–2017 ($N = 14$; 11–12 January 2017). (c) Nitrate to phosphate (μmol/L) and (d) silicic acid to nitrate (μmol/L) ratios for the upper 200 m in the Dalton, Mertz, and Ninnis polynyas during the 2016–2017 cruise. In (c) and (d), the linear regressions are indicated for each polynya. The dashed line in (c) indicates the Redfield ratio [16 N:1 P]. The dashed line in (d) indicates the Redfield ratio [1 Si:1 N] +45 for ease of comparison. (e) N* ($= NO_3^- - 16*PO_4^{3-}$; μmol/L) and (f) Si* ($= Si(OH)_4 - NO_3^-$; μmol/L) for the upper 200 m in the Dalton, Mertz, and Ninnis polynyas during the 2016–2017 cruise.

melt in the Mertz polynya, Shadwick et al. (2013) found that the change in icescape, following the calving of the Mertz Glacier Tongue, reduced the surface water salinity by 0.775 compared to summer 2008. This increase in sea ice melt and subsequent delivery of both ice algae and iron, which likely continued in the years following the calving of the Mertz Glacier Tongue, may have been responsible for the increase in primary productivity in the Mertz polynya postcalving (Shadwick et al., 2017). Our results contrast with
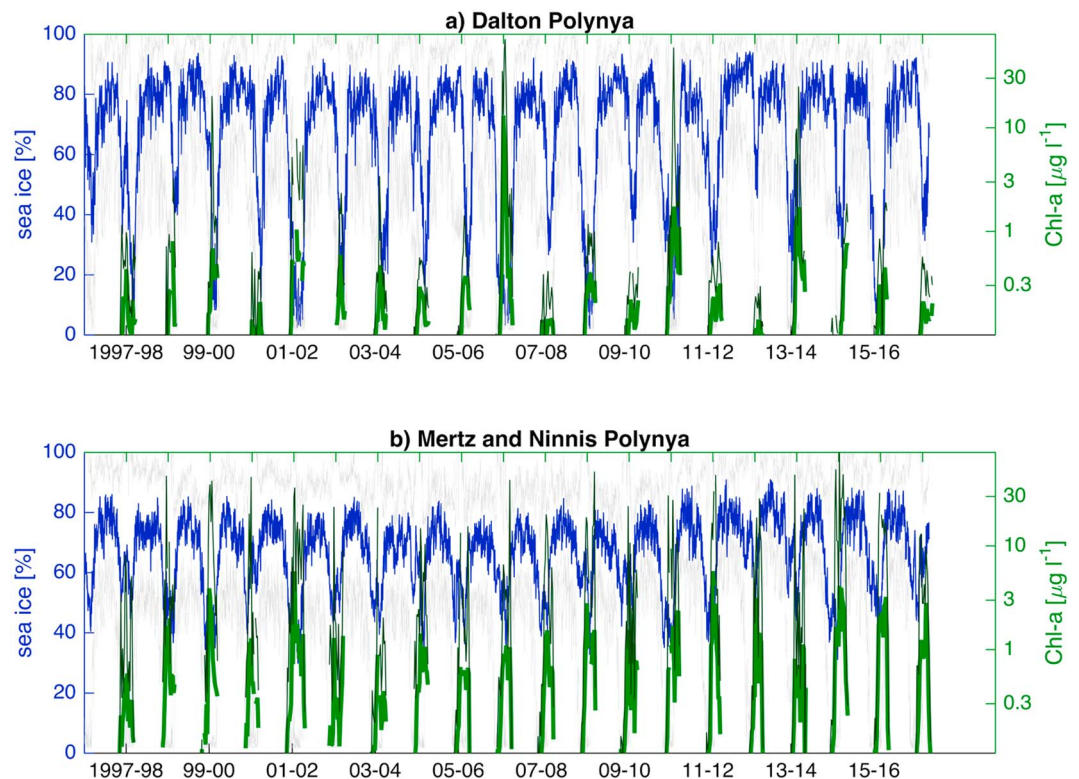
Figure 13. Satellite-derived daily sea ice concentration (%) and eight-day sea surface Chl *a* (µg/L) from 1997 to 2017 in (a) the Dalton polynya and (b) the Mertz and Ninnis polynyas. The average sea ice concentration is given in blue and the minimum and maximum in light gray. The average Chl *a* is given as a thick green line and the maximum Chl *a* as a thin green line.

those of Eveleth, Cassar, Sherrell, et al. (2017) who observed that, in 2012, 2013, and 2014, the summer NCP in the waters of the western Antarctic Peninsula was linearly related to the meteoric water content, but less so to the sea ice meltwater fraction. This difference may be explained by the strong changes in sea ice phenology which are taking place in west Antarctica compared to east Antarctica (Stammerjohn et al., 2012).

4.2.5. Phytoplankton Composition

In East Antarctica, phytoplankton communities are usually dominated by diatoms and *Phaeocystis* sp. in summer (December–January), before shifting to small flagellates in fall after nutrients have been exhausted (Davidson et al., 2010; Waters et al., 2000; Wright & van den Enden, 2000). Sambrotto et al. (2003) reported a prevalence of *Phaeocystis* east of the Mertz Glacier Tongue in December to January 2000–2001, coinciding with mixed layer depths between 20 and 50 m, while diatoms dominated everywhere else in the Mertz polynya where stratification was more pronounced. A large drawdown of silicic acid was consistently observed in the surface waters of the Mertz polynya during this and previous austral summer voyages to the region (Figure 12b). In the Ninnis polynya, the drawdown of silicic acid from the mixed layer was not as strong as in the Mertz (Figure 12b). And, in comparison, no silicic acid drawdown was observed in the Dalton polynya (Figure 12a). The strong depletion in surface silicic acid in the Mertz polynya suggests that diatoms were actively growing in the area at or prior to the time of our study, while a different community may have dominated in the Ninnis and Dalton polynyas.

The composition of the phytoplankton community was further elucidated by the nutrient ratios observed in the mixed layer. In the Mertz polynya, the slope of the N:P line was low (13.4; Figure 12c) but for Si:N it was high (1.5; Figure 12d), both of which are typical of diatom-dominated phytoplankton communities (Arrigo et al., 1999; Henley et al., 2017). In comparison, the high N:P (18.0) and low Si:N (0.2) slopes observed in the

Table 2

The 1997–2017 Summer (1 November to 28 February) Maximum and Average Satellite-Derived Chl a (µg/L) and Minimum and Average Sea Ice Concentration (%) in the Dalton and the Mertz and Ninnis Polynyas

Dalton Polynya

Years	Maximum Chl a	Average Chl a	Minimum Sea Ice	Average Sea Ice
1997–1998	1.15	0.17	14.50	45.70
1998–1999	3.24	0.20	34.64	75.79
1999–2000	20.21	0.32	29.72	51.86
2000–2001	0.63	0.08	37.68	74.16
2001–2002	7.85	0.42	17.62	35.55
2002–2003	2.35	0.21	36.85	66.83
2003–2004	3.42	0.16	26.34	60.44
2004–2005	0.56	0.16	24.67	60.61
2005–2006	1.42	0.19	32.68	74.39
2006–2007	71.47	2.05	14.43	27.09
2007–2008	0.41	0.10	32.52	68.66
2008–2009	1.18	0.23	19.59	40.37
2009–2010	0.40	0.11	42.98	76.81
2010–2011	59.48	0.62	13.93	37.30
2011–2012	0.79	0.17	21.65	51.92
2012–2013	0.30	0.08	49.09	83.28
2013–2014	24.98	0.54	16.84	45.45
2014–2015	1.26	0.20	31.11	68.71
2015–2016	1.90	0.21	13.49	33.52
2016–2017	0.57	0.13	39.07	77.46

Mertz and Ninnis polynyas

Years	Maximum Chl a	Average Chl a	Minimum sea ice	Average sea ice
1997–1998	8.21	0.28	8.29	58.03
1998–1999	47.59	0.67	7.26	50.26
1999–2000	42.57	1.11	5.78	43.31
2000–2001	46.34	0.45	7.52	57.39
2001–2002	36.50	1.36	6.81	48.64
2002–2003	23.81	0.37	4.96	54.22
2003–2004	23.43	0.28	6.98	52.75
2004–2005	14.80	0.59	6.92	57.04
2005–2006	15.48	0.42	6.50	52.46
2006–2007	43.27	0.57	7.02	54.85
2007–2008	20.13	0.58	7.24	51.33
2008–2009	52.14	0.93	8.15	56.98
2009–2010	24.16	0.53	9.57	58.13
2010–2011	30.66	0.99	11.42	44.76
2011–2012	48.39	1.21	14.28	51.05
2012–2013	28.70	0.73	20.15	66.50
2013–2014	48.64	0.47	22.80	63.58
2014–2015	80.56	1.63	8.40	45.72
2015–2016	32.37	1.35	7.53	52.42
2016–2017	13.07	0.82	8.38	58.75

Dalton polynya (Figures 12c and 12d) are typical of nondiatom phytoplankton communities and of lower latitudes (Martiny et al., 2013), and consistent with the absence of silicic acid drawdown in the mixed layer (Figure 12a). The fairly high N:P (17.9; Figure 12c) and low Si:N (0.5; Figure 12d) slopes observed in the Ninnis polynya together with the small drawdown of silicic acid in the mixed layer (Figure 12b) suggest a mixed phytoplankton community. These trends were confirmed by looking at the distribution of N* (= $NO_3^- - 16*PO_4^{3-}$) and Si* (= Si $(OH)_4 - NO_3^-$). N* decreased from the surface to 100 m in the Mertz and Ninnis polynyas, similarly to observations from the Antarctic Peninsula where diatoms are dominant (Henley et al., 2018), and unlike in the Dalton (Figure 12e). The increase of Si* from the

surface to 100 m in the Mertz polynya (Figure 12f) might indicate a faster remineralization of organic matter than the dissolution of biogenic silica (Henley et al., 2017). The differences in Si:N slopes, N*, and Si* between the polynyas could also be due to different nutrient ratios at the source, presumably deeper water masses, as well as iron-limited diatom communities (Assmy et al., 2013; Takeda, 1998). These trends were also confirmed by microscope analyses of the phytoplankton communities at the depths of the maximum Chl a concentration. In the Mertz polynya, the community was dominated by diatoms (*Fragilariopsis curta* and *F. cylindrus*). In the Ninnis polynya, the community was dominated by diatoms and small flagellates including *Phaeocystis antarctica*. In the Dalton polynya, the community was dominated by small flagellates including *P. antarctica*.

Finally, the absence of diatoms in the Dalton polynya is consistent with retrieved cores of diatomaceous oozes from this area (Leventer et al., 2014). In this study, the authors reported unusual floral assemblages in a Holocene diatom-rich sediment core retrieved from the midshelf. The diatoms species found there were typical of the open Southern Ocean, suggesting north-south advection of diatoms onto the shelf and the absence of diatoms in the polynya. In comparison, in the Mertz polynya, Sambrotto et al. (2003) observed geographical differences in silicic acid to NO_x deficit ratios, possibly reflecting geographical patterns of phytoplankton composition but also iron distribution. The authors argued that the correlation between iron and silicic acid to NO_x deficit ratios can be explained by the iron requirements for the reductive assimilation of nitrate. As a result, the most productive areas of the Mertz polynya, as shown by the authors' observations of surface water O_2 and $\Delta p CO_2$, corresponded to vigorous diatom growth at elevated iron levels (Sambrotto et al., 2003).

4.3. Implications for the Carbon Cycle: Air-Sea CO₂ Fluxes and Carbon Export

The spatial differences in phytoplankton biomass and primary productivity reported in the present study are consistent with the last 20 years of satellite estimates (Figure 13). During that period, the average satellite-derived phytoplankton biomass in the Dalton polynya was relatively high (>0.5 µg/L) for only a handful of years (2006–2007, 2010–2011, and 2013–2014; Figure 13a). These corresponded to low sea ice cover years (with an average summer concentration of 27, 37, and 45%, respectively; Table 2), although years with low sea ice cover did not always show high biomass (1997–1998, 2001–2002, 2008–2009, and 2015–2016; Table 2). Over the same period, the Mertz and Ninnis polynyas have comparatively been more productive (Figure 13b). In comparison, the average summer Chl a concentration was 4.1 ± 2.5 times higher in the Mertz and Ninnis polynyas than in the Dalton over the last 20 years (Table 2). Shadwick et al. (2013, 2017) showed that NCP in the Mertz polynya was twice as high postcalving (2012 and 2013) than precalving (2001 and 2008). This trend is confirmed by the satellite data as the mean Chl a in the Mertz and Ninnis polynyas was higher postcalving than during the 2002–2010 period (Figure 13b). In contrast, the period 1997–2001 was as productive as the present conditions. A detailed study of the sea ice and phytoplankton phenology as in Marchese et al. (2017) could confirm the long-term drivers of primary productivity in the three polynyas described in the present study.

In addition to being of paramount importance to top predators (Raymond et al., 2015), coastal Antarctic waters are large seasonal CO_2 sinks that correspond to the peak of the production season in summer (Arrigo, van Dijken, & Long, 2008; Moreau et al., 2012; Moreau et al., 2013; Mu et al., 2014; Roden et al., 2013; Shadwick et al., 2014), with a high potential to export organic carbon to the seafloor. As mentioned in section 1, the transfer of anthropogenic carbon to the ocean interior in coastal Antarctic environments such as polynyas could be significant to the global ocean CO_2 sink given the long residence time of AABW (1,000 years; England, 1995). In terms of carbon export to the seafloor, the continental shelf directly west of the Mertz Glacier Tongue is a site of heavy sedimentation of diatomaceous oozes, with sedimentation rates of ~300 cm/kyr (Dunbar et al., 2013), compared to ~53 cm/kyr in the South Atlantic Ocean (DeMaster, 1981). This emphasizes the potential importance of the biological pump of coastal Antarctic environments such as polynyas in the global carbon cycle.

5. Conclusion

Despite similarly optimal growing conditions (F_v/F_m), we observed significantly higher integrated phytoplankton biomass and nitrate-derived NCP in the Mertz and Ninnis polynyas compared to the Dalton

polynya. The most likely drivers were the shallow inflow of iron-rich modified Circumpolar Deep Water onto the shelf as well as a very large sea ice meltwater contribution. The productivity contrast between the three polynyas could not be explained by (1) the meteoric water fraction, (2) the presence of Ice Shelf Water, or (3) stratification of the mixed layer. In addition, we observed different phytoplankton communities between the polynyas. Diatoms were thriving in the Mertz and Ninnis polynyas but not in the Dalton polynya where *P. antarctica* dominated the community, with possible consequences for carbon export and higher trophic levels. Our study highlights how productivity of Antarctic coastal polynyas can vary strongly, reflecting physical drivers like input of sea ice melt or iron supply by mCDW. The impacts of climate change on Antarctic coastal productivity are therefore also likely to vary strongly with location and the nature of future changes in the ocean and cryosphere.

Appendix A
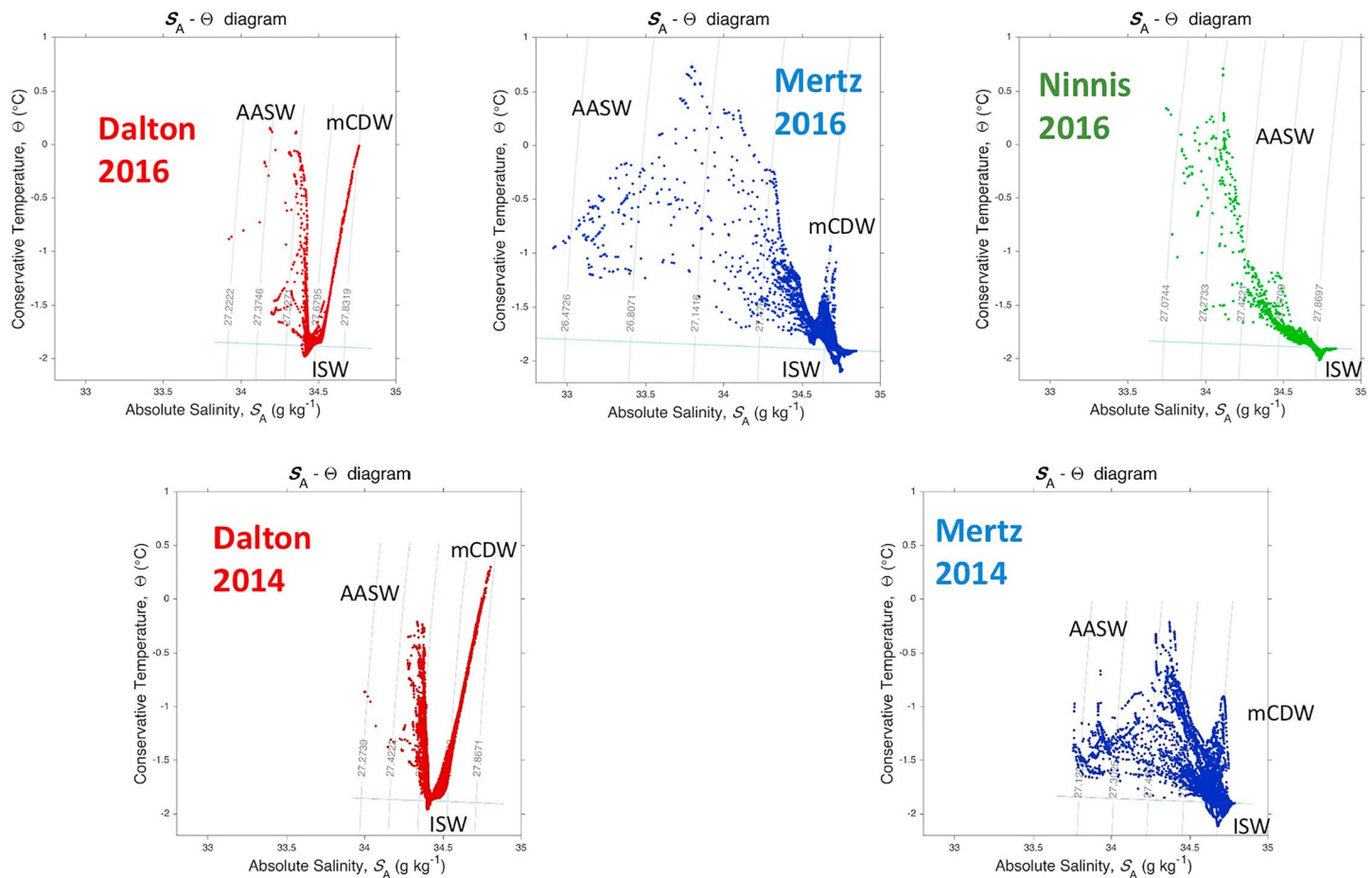
Figure A1. (top) Potential temperature (°C) versus salinity (g/kg) diagrams for CTD profiles from the Dalton, Mertz, and Ninnis polynyas (2016–2017 campaign). The presence of ice shelf water (ISW), Antarctic surface water (AASW), and modified circumpolar deep water (mCDW) are indicated. Potential density relative to the sea surface is contoured. (bottom) Potential temperature (°C) versus salinity (g/kg) for CTD profiles from the Dalton and Mertz polynyas for the 2014–2015 campaign as comparison.
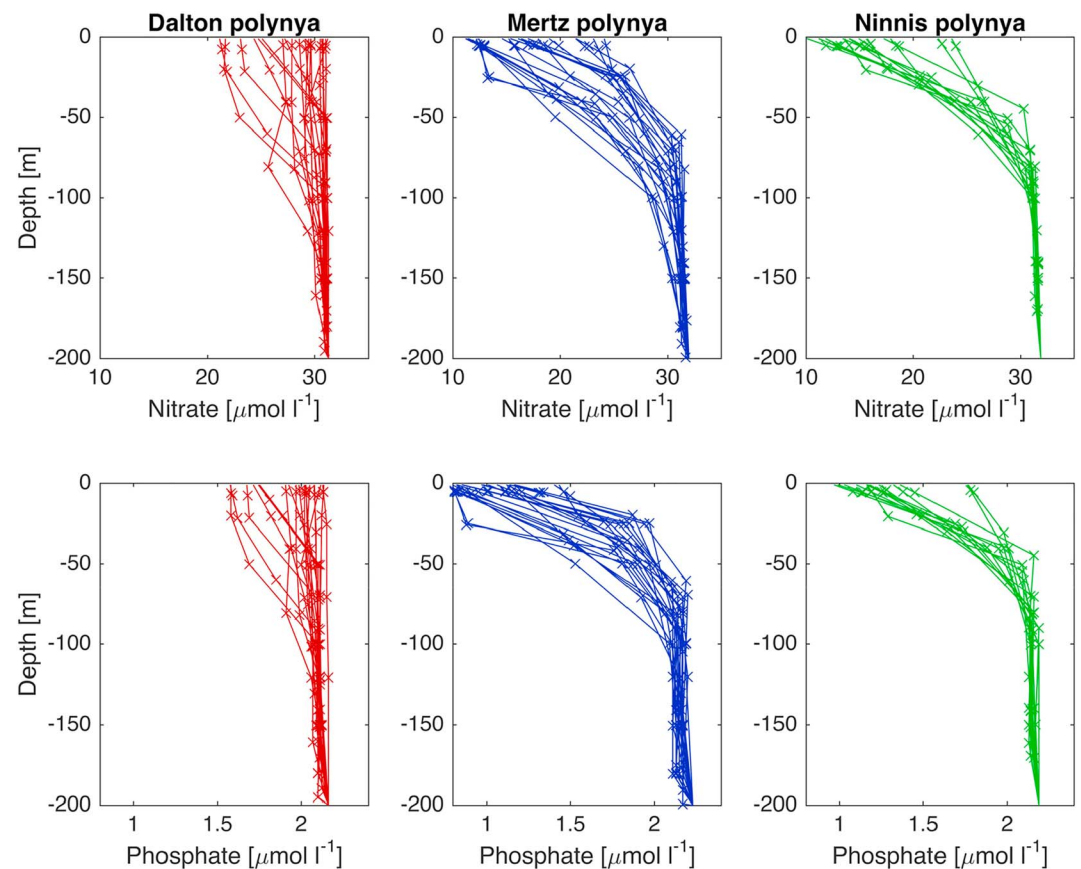
Figure A2. (top) Observed nitrate (μmol/L) and (bottom) phosphates (μmol/L) concentration (crosses) in the Dalton, Mertz, and Ninnis polynyas. The depth-integrated net community production (NCP) presented in Figure 7 was retrieved form the drawdown of nitrate concentrations presented here.

Contributions

S.M., D.L., and J.J. designed the original idea and are listed as first, second, and third authors. All other authors participated equally in writing the article and are ordered alphabetically. Additional contributions are as follows. Sampling was made possible thanks to D.L. and S.R.'s research voyages and interests in polynyas. Sampling for the biomass of phytoplankton was primarily carried out by S.M., J.J., D.L., and L.R. with additional support from V.P., M.R.M., M.C., and C.G. Primary productivity measurements were carried out by S.M. and M.A. and provided by B.T. Sampling for physical oceanography variables was carried out by E. C., B.L., M.R., and A.S. Calibration of the CTD data was performed by M.R.

References

Aoki, S., Kobayashi, R., Rintoul, S. R., Tamura, T., & Kusahara, K. (2017). Changes in water properties and flow regime on the continental shelf off the Adélie/George V Land coast, East Antarctica, after glacier tongue calving. *Journal of Geophysical Research: Oceans*, *122*, 6277–6294. https://doi.org/10.1002/2017JC012925

Armstrong, F. A. J., Stearns, C. R., & Strickland, J. D. H. (1967). The measurement of upwelling and subsequent biological process by means of the Technicon Autoanalyzer® and associated equipment. *Deep Sea Research and Oceanographic Abstracts*, *14*(3), 381–389. https://doi. org/10.1016/0011-7471(67)90082-4

Arrigo, K. R., Robinson, D. H., Dunbar, R. B., Leventer, A. R., & Lizotte, M. P. (2003). Physical control of chlorophyll *a*, POC, and TPN distributions in the pack ice of the Ross Sea, Antarctica. *Journal of Geophysical Research*, *108*(C10), 3316. https://doi.org/10.1029/ 2001JC001138

Arrigo, K. R., Robinson, D. H., Worthen, D. L., Dunbar, R. B., DiTullio, G. R., VanWoert, M., & Lizotte, M. P. (1999). Phytoplankton community structure and the drawdown of nutrients and CO_2 in the Southern Ocean. *Science*, *283*(5400), 365–367. https://doi.org/ 10.1126/science.283.5400.365

Arrigo, K. R., van Dijken, G., & Long, M. (2008). Coastal Southern Ocean: A strong anthropogenic CO_2 sink. *Geophysical Research Letters*, *35*, L21602. https://doi.org/10.1029/2008GL035624

Arrigo, K. R., van Dijken, G. L., & Bushinsky, S. (2008). Primary production in the Southern Ocean, 1997–2006. *Journal of Geophysical Research*, *113*, C08004. https://doi.org/10.1029/2007JC004551

Arrigo, K. R., van Dijken, G. L., & Strong, A. L. (2015). Environmental controls of marine productivity hot spots around Antarctica. *Journal of Geophysical Research: Oceans*, *120*, 5545–5565. https://doi.org/10.1002/2015JC010888

Assmy, P., Smetacek, V., Montresor, M., Klaas, C., Henjes, J., Strass, V. H., et al. (2013). Thick-shelled, grazer-protected diatoms decouple ocean carbon and silicon cycles in the iron-limited Antarctic Circumpolar Current. *Proceedings of the National Academy of Sciences*, *110*(51), 20,633–20,638. https://doi.org/10.1073/pnas.1309345110

Bertolin, M. L., & Schloss, I. R. (2009). Phytoplankton production after the collapse of the Larsen A Ice Shelf, Antarctica. *Polar Biology*, *32*(10), 1435–1446. https://doi.org/10.1007/s00300-009-0638-x

Buschmann, C. (1999). Photochemical and non-photochemical quenching coefficients of the chlorophyll fluorescence: Comparison of variation and limits. *Photosynthetica*, *37*(2), 217–224. https://doi.org/10.1023/A:1007003921135

Carvalho, F., Kohut, J., Oliver, M. J., & Schofield, O. (2017). Defining the ecologically relevant mixed-layer depth for Antarctica's coastal seas. *Geophysical Research Letters*, *44*, 338–345. https://doi.org/10.1002/2016GL071205

Cassar, N., Barnett, B. A., Bender, M. L., Kaiser, J., Hamme, R. C., & Tilbrook, B. (2009). Continuous high-frequency dissolved O_2/Ar measurements by equilibrator inlet mass spectrometry. *Analytical Chemistry*, *81*(5), 1855–1864. https://doi.org/10.1021/ac802300u

Cassar, N., Nevison, C. D., & Manizza, M. (2014). Correcting oceanic O_2/Ar-net community production estimates for vertical mixing using N_2O observations. *Geophysical Research Letters*, *41*, 8961–8970. https://doi.org/10.1002/2014GL062040

Cavalieri, D., Parkinson, C., Gloersen, P., & Zwally, H. J. (2008). *Sea Ice Concentrations From Nimbus-7 SMMR and DMSP SSM/I Passive Microwave Data, [1978–2007]*. Boulder, CO: National Snow and Ice Data Center. Digital media

Constable, A. J., Melbourne-Thomas, J., Corney, S. P., Arrigo, K. R., Barbraud, C., Barnes, D. K. A., et al. (2014). Climate change and Southern Ocean ecosystems I: How changes in physical habitats directly affect marine biota. *Global Change Biology*, *20*(10), 3004–3025. https://doi.org/10.1111/gcb.12623

Davidson, A. T., Scott, F. J., Nash, G. V., Wright, S. W., & Raymond, B. (2010). Physical and biological control of protistan community composition, distribution and abundance in the seasonal ice zone of the Southern Ocean between 30 and 80°E. *Deep Sea Research Part II: Topical Studies in Oceanography*, *57*(9), 828–848. https://doi.org/10.1016/j.dsr2.2009.02.011

de Jong, J., Schoemann, V., Lannuzel, D., Croot, P., de Baar, H., & Tison, J.-L. (2012). Natural iron fertilization of the Atlantic sector of the Southern Ocean by continental shelf sources of the Antarctic Peninsula. *Journal of Geophysical Research*, *117*, G01029. https://doi.org/10.1029/2011JG001679

de Jong, J., Schoemann, V., Maricq, N., Mattielli, N., Langhorne, P., Haskell, T., & Tison, J.-L. (2013). Iron in land-fast sea ice of McMurdo Sound derived from sediment resuspension and wind-blown dust attributes to primary productivity in the Ross Sea, Antarctica. *Marine Chemistry*, *157*(Supplement C), 24–40. https://doi.org/10.1016/j.marchem.2013.07.001

DeMaster, D. J. (1981). The supply and accumulation of silica in the marine environment. *Geochimica et Cosmochimica Acta*, *45*(10), 1715–1732. https://doi.org/10.1016/0016-7037(81)90006-5

Dunbar, R. B., Anderson, J. B., Domack, E. W., & Jacobs, S. S. (2013). Oceanographic influences on sedimentation along the Antarctic continental shelf. In *Oceanology of the Antarctic Continental Shelf* (pp. 291–312). Washington, DC: American Geophysical Union. https://doi.org/10.1029/AR043p0291

Duprat, L. P. A. M., Bigg, G. R., & Wilton, D. J. (2016). Enhanced Southern Ocean marine productivity due to fertilization by giant icebergs. *Nature Geoscience*, *9*(3), 219–221. https://doi.org/10.1038/ngeo2633

Dutrieux, P., Rydt, J. D., Jenkins, A., Holland, P. R., Ha, H. K., Lee, S. H., et al. (2014). Strong sensitivity of Pine Island ice-shelf melting to climatic variability. *Science*, *343*(6167), 174–178. https://doi.org/10.1126/science.1244341

England, M. H. (1995). The age of water and ventilation timescales in a global ocean model. *Journal of Physical Oceanography*, *25*(11), 2756–2777. https://doi.org/10.1175/1520-0485(1995)025<2756:TAOWAV>2.0.CO;2

Eveleth, R., Cassar, N., Doney, S. C., Munro, D. R., & Sweeney, C. (2017). Biological and physical controls on O_2/Ar, Ar and pCO₂ variability at the Western Antarctic Peninsula and in the Drake Passage. *Deep Sea Research Part II: Topical Studies in Oceanography*, *139*, 77–88. https://doi.org/10.1016/j.dsr2.2016.05.002

Eveleth, R., Cassar, N., Sherrell, R. M., Ducklow, H., Meredith, M. P., Venables, H. J., et al. (2017). Ice melt influence on summertime net community production along the Western Antarctic Peninsula. *Deep Sea Research Part II: Topical Studies in Oceanography*, *139*, 89–102. https://doi.org/10.1016/j.dsr2.2016.07.016

Ferreyra, G., Schloss, I., & Demers, S. (2004). Rôle de la glace saisonnière dans la dynamique de l'écosystème marin de l'Antarctique: Impact potentiel du changement climatique global. *VertigO - La revue en sciences de l'environnement*, *5*(3), 1–11.

Fritz, J. J., Neale, P. J., Davis, R. F., & Peloquin, J. A. (2008). Response of Antarctic phytoplankton to solar UVR exposure: Inhibition and recovery of photosynthesis in coastal and pelagic assemblages. *Marine Ecology Progress Series*, *365*, 1–16. https://doi.org/10.3354/meps07610

Gerringa, L. J. A., Alderkamp, A.-C., Laan, P., Thuróczy, C.-E., De Baar, H. J. W., Mills, M. M., et al. (2012). Iron from melting glaciers fuels the phytoplankton blooms in Amundsen Sea (Southern Ocean): Iron biogeochemistry. *Deep Sea Research Part II: Topical Studies in Oceanography*, *71-76*, 16–31. https://doi.org/10.1016/j.dsr2.2012.03.007

Grotti, M., Soggia, F., Ianni, C., & Frache, R. (2005). Trace metals distributions in coastal sea ice of Terra Nova Bay, Ross Sea, Antarctica. *Antarctic Science*, *17*(2), 289–300. https://doi.org/10.1017/S0954102005002695

Henley, S. F., Jones Elizabeth, M., Venables Hugh, J., Meredith Michael, P., Firing Yvonne, L., Dittrich, R., et al. (2018). Macronutrient and carbon supply, uptake and cycling across the Antarctic Peninsula shelf during summer. *Philosophical Transactions of the Royal Society A: Mathematical, Physical and Engineering Sciences*, *376*(2122). https://doi.org/10.1098/rsta.2017.0168

Henley, S. F., Tuerena, R. E., Annett, A. L., Fallick, A. E., Meredith, M. P., Venables, H. J., et al. (2017). Macronutrient supply, uptake and recycling in the coastal ocean of the west Antarctic Peninsula. *Deep Sea Research Part II: Topical Studies in Oceanography*, *139*, 58–76. https://doi.org/10.1016/j.dsr2.2016.10.003

Herraiz-Borreguero, L., Lannuzel, D., van der Merwe, P., Treverrow, A., & Pedro, J. B. (2016). Large flux of iron from the Amery Ice Shelf marine ice to Prydz Bay, East Antarctica. *Journal of Geophysical Research: Oceans*, *121*, 6009–6020. https://doi.org/10.1002/2016JC011687

Heywood, K. J., Schmidtko, S., Heuze, C., Kaiser, J., Jickells, T. D., Queste, B. Y., et al. (2014). Ocean processes at the Antarctic continental slope. *Philosophical Transactions of the Royal Society A: Mathematical, Physical and Engineering Sciences*, *372*(2019). https://doi.org/10.1098/rsta.2013.0047

Holm-Hansen, O., Lorenzen, C. J., Holmes, R. W., & Strickland, J. D. H. (1965). Fluorometric determination of chlorophyll. *Journal du Conseil*, *30*(1), 3–15. https://doi.org/10.1093/icesjms/30.1.3

Kalnay, E., Kanamitsu, M., Kistler, R., Collins, W., Deaven, D., Gandin, L., et al. (1996). The NCEP/NCAR 40-year reanalysis project. *Bulletin of the American Meteorological Society*, 77(3), 437–471. https://doi.org/10.1175/1520-0477(1996)077<0437:TNYRP>2.0.CO;2

Karnovsky, N., Ainley, D. G., & Lee, P. (2007). Chapter 12 the impact and importance of production in polynyas to top-trophic predators: Three case histories. In W. O. Smith & D. G. Barber (Eds.), *Elsevier Oceanography Series* (pp. 391–410). Elsevier. https://doi.org/10.1016/S0422-9894(06)74012-0

Karstensen, J., Schütte, F., Pietri, A., Krahmann, G., Fiedler, B., Grundle, D., et al. (2017). Upwelling and isolation in oxygen-depleted anticyclonic modewater eddies and implications for nitrate cycling. *Biogeosciences*, 14(8), 2167–2181. https://doi.org/10.5194/bg-14-2167-2017

Kaufman, D. E., Friedrichs, M. A. M., Smith, W. O., Queste, B. Y., & Heywood, K. J. (2014). Biogeochemical variability in the southern Ross Sea as observed by a glider deployment. *Deep Sea Research Part I: Oceanographic Research Papers*, 92, 93–106. https://doi.org/10.1016/j.dsr.2014.06.011

Kérouel, R., & Aminot, A. (1997). Fluorometric determination of ammonia in sea and estuarine waters by direct segmented flow analysis. *Marine Chemistry*, 57(3), 265–275. https://doi.org/10.1016/S0304-4203(97)00040-6

Khatiwala, S., Primeau, F., & Hall, T. (2009). Reconstruction of the history of anthropogenic CO_2 concentrations in the ocean. *Nature*, 462(7271), 346–349. https://doi.org/10.1038/nature08526, https://www.nature.com/articles/nature08526#supplementary-information

Kirk, J. T. O. (1994). *Light and Photosynthesis in Aquatic Systems* (p. 401). Cambridge: Cambridge University Press. https://doi.org/10.1017/CBO9780511623370

Landschützer, P., Gruber, N., Haumann, F. A., Rödenbeck, C., Bakker, D. C. E., van Heuven, S., et al. (2015). The reinvigoration of the Southern Ocean carbon sink. *Science*, 349(6253), 1221–1224. https://doi.org/10.1126/science.aab2620

Lannuzel, D., Chever, F., van der Merwe, P. C., Janssens, J., Roukaerts, A., Cavagna, A.-J., et al. (2016). Iron biogeochemistry in Antarctic pack ice during SIPEX-2. *Deep Sea Research Part II: Topical Studies in Oceanography*, 131, 111–122. https://doi.org/10.1016/j.dsr2.2014.12.003

Lannuzel, D., Schoemann, V., de Jong, J., Chou, L., Delille, B., Becquevort, S., & Tison, J. L. (2008). Iron study during a time series in the western Weddell pack ice. *Marine Chemistry*, 108(1–2), 85–95. https://doi.org/10.1016/j.marchem.2007.10.006

Lannuzel, D., Schoemann, V., De Jong, J., Pasquer, B., Van Der Merwe, P., Masson, F., et al. (2010). Distribution of dissolved iron in Antarctic Sea ice: Spatial, seasonal, and inter-annual variability. *Journal of Geophysical Research*, 115, G03022. https://doi.org/10.1029/2009JG001031

Lannuzel, D., Vancoppenolle, M., van der Merwe, P., de Jong, J., Meiners, K. M., Grotti, M., et al. (2016). Iron in sea ice: Review and new insights. *Elementa: Science of the Anthropocene*, 4(000130). https://doi.org/10.12952/journal.elementa.000130

Laws, E. A. (1991). Photosynthetic quotients, new production and net community production in the open ocean. *Deep Sea Research Part A. Oceanographic Research Papers*, 38(1), 143–167. https://doi.org/10.1016/0198-0149(91)90059-O

Le Quéré, C., Andrew, R. M., Canadell, J. G., Sitch, S., Korsbakken, J. I., Peters, G. P., et al. (2016). Global carbon budget 2016. *Earth System Science Data*, 8(2), 605–649. https://doi.org/10.5194/essd-8-605-2016

Lenton, A., Tilbrook, B., Law, R. M., Bakker, D., Doney, S. C., Gruber, N., et al. (2013). Sea–air CO_2 fluxes in the Southern Ocean for the period 1990–2009. *Biogeosciences*, 10(6), 4037–4054. https://doi.org/10.5194/bg-10-4037-2013

Leventer, A., Armand, L., Redovian, M., Domack, E. W., Shevenell, A., Smith, C., et al. (2014). *Holocene Sedimentary Record of Unusual Primary Productivity, Dalton Polynya, Sabrina Coast, East Antarctica*. San Francisco, USA: American Geophysical Union, edited.

Lin, H., Rauschenberg, S., Hexel, C. R., Shaw, T. J., & Twining, B. S. (2011). Free-drifting icebergs as sources of iron to the Weddell Sea. *Deep Sea Research Part II: Topical Studies in Oceanography*, 58(11-12), 1392–1406. https://doi.org/10.1016/j.dsr2.2010.11.020

Lorenzen, C. J. (1966). A method for the continuous measurement of in vivo chlorophyll concentration. *Deep Sea Research and Oceanographic Abstracts*, 13(2), 223–227. https://doi.org/10.1016/0011-7471(66)91102-8

Marchese, C., Albouy, C., Tremblay, J.-É., Dumont, D., D'Ortenzio, F., Vissault, S., & Bélanger, S. (2017). Changes in phytoplankton bloom phenology over the North Water (NOW) polynya: a response to changing environmental conditions. *Polar Biology*(1–17, 40(9), 1721–1737. https://doi.org/10.1007/s00300-017-2095-2

Marinov, I., Gnanadesikan, A., Toggweiler, J. R., & Sarmiento, J. L. (2006). The Southern Ocean biogeochemical divide. *Nature*, 441(7096), 964–967. http://www.nature.com/nature/journal/v441/n7096/suppinfo/nature04883_S1.html, https://doi.org/10.1038/nature04883

Martin, J. H., Gordon, R. M., & Fitzwater, S. E. (1990). Iron in Antarctic waters. *Nature*, 345(6271), 156–158. https://doi.org/10.1038/345156a0

Martiny, A. C., Pham, C. T. A., Primeau, F. W., Vrugt, J. A., Moore, J. K., Levin, S. A., & Lomas, M. W. (2013). Strong latitudinal patterns in the elemental ratios of marine plankton and organic matter. *Nature Geoscience*, 6(4), 279–283. https://doi.org/10.1038/ngeo1757, https://www.nature.com/articles/ngeo1757#supplementary-information

Massom, R. A., Harris, P. T., Michael, K. J., & Potter, M. J. (1998). The distribution and formative processes of latent-heat polynyas in East Antarctica. *Annals of Glaciology*, 27(1), 420–426. https://doi.org/10.3198/1998AoG27-1-420-426

Measures, C. I., Brown, M. T., Selph, K. E., Apprill, A., Zhou, M., Hatta, M., & Hiscock, W. T. (2013). The influence of shelf processes in delivering dissolved iron to the HNLC waters of the Drake Passage, Antarctica. *Deep Sea Research Part II: Topical Studies in Oceanography*, 90(Supplement C), 77–88. https://doi.org/10.1016/j.dsr2.2012.11.004

Meredith, M. P., Brandon, M. A., Wallace, M. I., Clarke, A., Leng, M. J., Renfrew, I. A., et al. (2008). Variability in the freshwater balance of northern Marguerite Bay, Antarctic Peninsula: Results from δ^{18}O. *Deep Sea Research Part II: Topical Studies in Oceanography*, 55(3-4), 309–322. https://doi.org/10.1016/j.dsr2.2007.11.005

Moore, C. M., Mills, M. M., Arrigo, K. R., Berman-Frank, I., Bopp, L., Boyd, P. W., et al. (2013). Processes and patterns of oceanic nutrient limitation. *Nature Geoscience*, 6(9), 701–710. https://doi.org/10.1038/ngeo1765

Moreau, S., Fiori, E. D., Schloss, I. R., Almandoz, G. O., Esteves, J. L., Paparazzo, F. E., & Ferreyra, G. A. (2013). The role of phytoplankton composition and microbial community metabolism in sea–air $\Delta p CO_2$ variation in the Weddell Sea. *Deep Sea Research Part I: Oceanographic Research Papers*, 82, 44–59. https://doi.org/10.1016/j.dsr.2013.07.010

Moreau, S., Mostajir, B., Bélanger, S., Schloss, I. R., Vancoppenolle, M., Demers, S., & Ferreyra, G. A. (2015). Climate change enhances primary production in the western Antarctic Peninsula. *Global Change Biology*, 21(6), 2191–2205. https://doi.org/10.1111/gcb.12878

Moreau, S., Schloss, I. R., Mostajir, B., Demers, S., Almandoz, G. O., Ferrario, M. E., & Ferreyra, G. A. (2012). Influence of microbial community composition and metabolism on air-sea $\Delta p CO_2$ variation off the western Antarctic Peninsula. *Marine Ecology Progress Series*, 446, 45–59. https://doi.org/10.3354/meps09466

Mu, L., Stammerjohn, S. E., Lowry, K. E., & Yager, P. L. (2014). Spatial variability of surface $p CO_2$ and air-sea CO_2 flux in the Amundsen Sea Polynya, Antarctica. *Elementa: Science of the Anthropocene*, 2. https://doi.org/10.12952/journal.elementa.000036

Murphy, J., & Riley, J. P. (1962). A modified single solution method for the determination of phosphate in natural waters. *Analytica Chimica Acta*, *27*, 31–36. https://doi.org/10.1016/S0003-2670(00)88444-5

Ohshima, K. I., Nihashi, S., & Iwamoto, K. (2016). Global view of sea-ice production in polynyas and its linkage to dense/bottom water formation. *Geoscience Letters*, *3*(1), 13. https://doi.org/10.1186/s40562-016-0045-4

Paolo, F. S., Fricker, H. A., & Padman, L. (2015). Volume loss from Antarctic ice shelves is accelerating. *Science*, *348*(6232), 327–331. https://doi.org/10.1126/science.aaa0940

Peck, L. S., Barnes, D. K. A., Cook, A. J., Fleming, A. H., & Clarke, A. (2010). Negative feedback in the cold: Ice retreat produces new carbon sinks in Antarctica. *Global Change Biology*, *16*(9), 2614–2623. https://doi.org/10.1111/j.1365-2486.2009.02071.x

Periard, C., & Pettre, P. (1993). Some aspects of the climatology of Dumont d'Urville, Adélie land, Antarctica. *International Journal of Climatology*, *13*(3), 313–328. https://doi.org/10.1002/joc.3370130307

Raiswell, R., Benning, L. G., Tranter, M., & Tulaczyk, S. (2008). Bioavailable iron in the Southern Ocean: The significance of the iceberg conveyor belt. *Geochemical Transactions*, *9*(1), 7–9. https://doi.org/10.1186/1467-4866-9-7

Raymond, B., Lea, M. A., Patterson, T., Andrews-Goff, V., Sharples, R., Charrassin, J. B., et al. (2015). Important marine habitat off East Antarctica revealed by two decades of multi-species predator tracking. *Ecography*, *38*(2), 121–129. https://doi.org/10.1111/ecog.01021

Redfield, A. C., Ketchum, B. H., & Richards, F. A. (1963). The influence of organisms on the composition of seawater. In M. N. Hill (Ed.), *The Sea* (pp. 26–77). New York: Interscience.

Rees, C., Pender, L., Sherrin, K., Schwanger, C., Hughes, P., Tibben, S., et al. (2019). Methods for reproducible shipboard SFA nutrient measurement using RMNS and automated data processing. *Limnology and Oceanography: Methods*, *17*(1), 25–41. https://doi.org/10.1002/lom3.10294

Reuer, M. K., Barnett, B. A., Bender, M. L., Falkowski, P. G., & Hendricks, M. B. (2007). New estimates of Southern Ocean biological production rates from O_2/Ar ratios and the triple isotope composition of O_2. *Deep Sea Research (Part I, Oceanographic Research Papers)*, *54*(6), 951–974. https://doi.org/10.1016/j.dsr.2007.02.007

Rignot, E., Jacobs, S., Mouginot, J., & Scheuchl, B. (2013). Ice-shelf melting around Antarctica. *Science*, *341*(6143), 266–270. https://doi.org/10.1126/science.1235798

Rignot, E., & Jacobs, S. S. (2002). Rapid bottom melting widespread near Antarctic ice sheet grounding lines. *Science*, *296*(5575), 2020–2023. https://doi.org/10.1126/science.1070942

Rintoul, S. R. (1998). On the origin and influence of Adelie land bottom water. *Antarctic Research Series*, *75*, 151–171. https://doi.org/10.1029/AR075p0151

Rintoul, S. R., Silvano, A., Pena-Molino, B., van Wijk, E., Rosenberg, M., Greenbaum, J. S., & Blankenship, D. D. (2016). Ocean heat drives rapid basal melt of the Totten Ice Shelf. *Science Advances*, *2*(12), e1601610. https://doi.org/10.1126/sciadv.1601610

Roden, N. P., Shadwick, E. H., Tilbrook, B., & Trull, T. W. (2013). Annual cycle of carbonate chemistry and decadal change in coastal Prydz Bay, East Antarctica. *Marine Chemistry*, *155*, 135–147. https://doi.org/10.1016/j.marchem.2013.06.006

Rosenberg, M., & Rintoul, S. (2010). *Aurora Australis* marine science cruises AU0803 and AU0806: Oceanographic field measurements and analysis*Rep.*, Hobart, Australia.

Rosenberg, M., & Rintoul, S. (2011). *Aurora Australis* Marine Science Cruise AU1121—Oceanographic Field Measurements and analysis*Rep.*, Hobart, Australia.

Rosenberg, M., & Rintoul, S. (2012). *Aurora Australis* Marine Science Cruise AU1203—Oceanographic Field Measurements and analysis*Rep.*, Hobart, Australia.

Rosenberg, M., & Rintoul, S. (2016). *Aurora Australis* marine science cruise AU1402, Totten and Mertz CTDs and moorings—Oceanographic field measurements and analysis*Rep.*, Hobart, Australia.

Rosenberg, M., & Rintoul, S. (2017). *Aurora Australis* marine science cruise AU1602, Dalton, Mertz and Ninnis CTD's—Oceanographic field measurements and analysis. *Rep.*, 33 pp, ACE-CRC, Hobart, 2017.

Sabine, C. L., Feely, R. A., Gruber, N., Key, R. M., Lee, K., Bullister, J. L., et al. (2004). The oceanic sink for anthropogenic CO_2. *Science*, *305*(5682), 367–371. https://doi.org/10.1126/science.1097403

Sallee, J.-B., Matear, R. J., Rintoul, S. R., & Lenton, A. (2012). Localized subduction of anthropogenic carbon dioxide in the Southern Hemisphere oceans. *Nature Geoscience*, *5*(8), 579–584. https://doi.org/10.1038/ngeo1523

Sambrotto, R. N., Matsuda, A., Vaillancourt, R., Brown, M., Langdon, C., Jacobs, S. S., & Measures, C. (2003). Summer plankton production and nutrient consumption patterns in the Mertz Glacier Region of East Antarctica. *Deep Sea Research Part II: Topical Studies in Oceanography*, *50*(8–9), 1393–1414. https://doi.org/10.1016/S0967-0645(03)00076-6

Schreiber, U. (2004). Pulse-amplitude-modulation (PAM) fluorometry and saturation pulse method: An overview. In G. C. Papageorgiou, & Govindjee (Eds.), *Chlorophyll a Fluorescence: A Signature of Photosynthesis* (pp. 279–319). Dordrecht, Netherlands: Springer. https://doi.org/10.1007/978-1-4020-3218-9_11

Sedwick, P. N., Bowie, A. R., & Trull, T. W. (2008). Dissolved iron in the Australian sector of the Southern Ocean (CLIVAR SR3 section): Meridional and seasonal trends. *Deep Sea Research Part I: Oceanographic Research Papers*, *55*(8), 911–925. https://doi.org/10.1016/j.dsr.2008.03.011

Shadwick, E. H., Rintoul, S. R., Tilbrook, B., Williams, G. D., Young, N., Fraser, A. D., et al. (2013). Glacier tongue calving reduced dense water formation and enhanced carbon uptake. *Geophysical Research Letters*, *40*, 904–909. https://doi.org/10.1002/grl.50178

Shadwick, E. H., Tilbrook, B., & Currie, K. I. (2017). Late-summer biogeochemistry in the Mertz polynya: East Antarctica. *Journal of Geophysical Research: Oceans*, *122*, 7380–7394. https://doi.org/10.1002/2017JC013015

Shadwick, E. H., Tilbrook, B., & Williams, G. D. (2014). Carbonate chemistry in the Mertz polynya (East Antarctica): Biological and physical modification of dense water outflows and the export of anthropogenic CO_2. *Journal of Geophysical Research: Oceans*, *119*, 1–14. https://doi.org/10.1002/2013JC009286

Sherrell, R. M., Lagerström, M. E., Forsch, K. O., Stammerjohn, S. E., & Yager, P. L. (2015). Dynamics of dissolved iron and other bioactive trace metals (Mn, Ni, Cu, Zn) in the Amundsen Sea Polynya, Antarctica. *Elementa: Science of the Anthropocene*, *3*, 000071. https://doi.org/10.12952/journal.elementa.000071

Sigman, D. M., Hain, M. P., & Haug, G. H. (2010). The polar ocean and glacial cycles in atmospheric CO_2 concentration. *Nature*, *466*(7302), 47–55. https://doi.org/10.1038/nature09149

Silvano, A., Rintoul, S. R., & Herraiz-Borreguero, L. (2016). Ocean-ice shelf interaction in East Antarctica. *Oceanography*, *29*(4), 130–143. https://doi.org/10.5670/oceanog.2016.105

Silvano, A., Rintoul, S. R., Peña-Molino, B., Hobbs, W. R., van Wijk, E., Aoki, S., et al. (2018). Freshening by glacial meltwater enhances melting of ice shelves and reduces formation of Antarctic Bottom Water. *Science Advances*, *4*(4), eaap9467. https://doi.org/10.1126/sciadv.aap9467

Silvano, A., Rintoul, S. R., Peña-Molino, B., & Williams, G. D. (2017). Distribution of water masses and meltwater on the continental shelf near the Totten and Moscow University ice shelves. *Journal of Geophysical Research: Oceans*, *122*, 2050–2068. https://doi.org/10.1002/2016JC012115

Snow, K., Rintoul, S. R., Sloyan, B. M., & Hogg, A. M. (2018). Change in dense shelf water and Adélie land bottom water precipitated by iceberg calving. *Geophysical Research Letters*, *45*, 2380–2387. https://doi.org/10.1002/2017GL076195

Stammerjohn, S., Massom, R., Rind, D., & Martinson, D. (2012). Regions of rapid sea ice change: An inter-hemispheric seasonal comparison. *Geophysical Research Letters*, *39*, L06501. https://doi.org/10.1029/2012GL050874

Tagliabue, A., Bowie, A. R., Boyd, P. W., Buck, K. N., Johnson, K. S., & Saito, M. A. (2017). The integral role of iron in ocean biogeochemistry. *Nature*, *543*(7643), 51–59. https://doi.org/10.1038/nature21058

Takahashi, T., Sutherland, S. C., Wanninkhof, R., Sweeney, C., Feely, R. A., Chipman, D. W., et al. (2009). Climatological mean and decadal change in surface ocean pCO_2, and net sea-air CO_2 flux over the global oceans. *Deep-Sea Research (Part II, Topical Studies in Oceanography)*, *56*(8–10), 554–577. https://doi.org/10.1016/j.dsr2.2008.12.009

Takeda, S. (1998). Influence of iron availability on nutrient consumption ratio of diatoms in oceanic waters. *Nature*, *393*(6687), 774–777. https://doi.org/10.1038/31674

Tamura, T., Williams, G. D., Fraser, A. D., & Ohshima, K. I. (2012). Potential regime shift in decreased sea ice production after the Mertz Glacier calving. *Nature Communications*, *3*(1), 826. https://doi.org/10.1038/ncomms1820

Vaillancourt, R. D., Sambrotto, R. N., Green, S., & Matsuda, A. (2003). Phytoplankton biomass and photosynthetic competency in the summertime Mertz glacier region of East Antarctica. *Deep Sea Research Part II: Topical Studies in Oceanography*, *50*(8–9), 1415–1440. http://doi.org/10.1016/S0967-0645(03)00077-8

Wanninkhof, R. (2014). Relationship between wind speed and gas exchange over the ocean revisited. *Limnology and Oceanography: Methods*, *12*(6), 351–362. https://doi.org/10.4319/lom.2014.12.351

Waters, R. L., van den Enden, R., & Marchant, H. J. (2000). Summer microbial ecology off East Antarctica (80–150°E): protistan community structure and bacterial abundance. *Deep Sea Research Part II: Topical Studies in Oceanography*, *47*(12), 2401–2435. https://doi.org/10.1016/S0967-0645(00)00030-8

Williams, G. D., Meijers, A. J. S., Poole, A., Mathiot, P., Tamura, T., & Klocker, A. (2011). Late winter oceanography off the Sabrina and BANZARE coast (117–128°E), East Antarctica. *Deep Sea Research Part II: Topical Studies in Oceanography*, *58*(9–10), 1194–1210. https://doi.org/10.1016/j.dsr2.2010.10.035

Wood, E. D., Armstrong, F. A. J., & Richards, F. A. (1967). Determination of nitrate in seawater by cadmium-copper reduction to nitrite. *Journal of theMarine Biological Association of U.K.*, *47*(01), 23–31. https://doi.org/10.1017/S002531540003352X

Wright, A. P., Young, D. A., Roberts, J. L., Schroeder, D. M., Bamber, J. L., Dowdeswell, J. A., et al. (2012). Evidence of hydrological connection between the ice divide and ice sheet margin in the Aurora Subglacial Basin, East Antarctica. *Journal of Geophysical Research*, *117*, F01033. https://doi.org/10.1029/2011JF002066

Wright, S. W., & van den Enden, R. L. (2000). Phytoplankton community structure and stocks in the East Antarctic marginal ice zone (BROKE survey, January–March 1996) determined by CHEMTAX analysis of HPLC pigment signatures. *Deep Sea Research Part II: Topical Studies in Oceanography*, *47*(12–13), 2363–2400. http://doi.org/10.1016/S0967-0645(00)00029-1

Young, N., Legrésy, B., Coleman, R., & Massom, R. (2010). Mertz glacier tongue unhinged by giant iceberg. *Australian Antarctic Magazine*, *19*(18).